Alma Mater Studiorum - Università di Bologna

SCUOLA DI SCIENZE

Dipartimento di Chimica Industriale "Toso Montanari"

Corso di Laurea Magistrale in

Chimica Industriale

Curriculum: Advanced Spectroscopy in Chemistry

Classe LM-71 - Scienze e Tecnologie della Chimica Industriale

3D electrocatalysts for the selective glucose oxidation

Tesi di laurea sperimentale

CANDIDATO

Nicola Poli

RELATORE

Chiar.mo Prof. Giuseppe Fornasari

CORRELATORE

Prof. ssa Patricia Benito Martìn

Dott. Giancosimo Sanghez De Luna

Anno Accademico 2018-2019

Keywords

D-Glucose

Open-cell Ni metal foam

Electrochemical oxidation

Gluconic acid

Glucaric acid

Summary

Aim of the work .....

1. Introduction 1

1.1 Biomass 2

1.1.1 Lignocellulosic biomass 3

1.2 Biorefinery 5

1.3 Lignocellulosic biomass pre-treatment 8

1.3.1 Physical Treatment 8

1.3.2 Physico-Chemical Treatment 9

1.3.3 Chemical Pretreatments 11

1.4 Hydrolytic processes for the glucose production 13

1.5 Glucose and its derivatives 14

1.6 Oxidation products of the glucose 16

1.6.1 Gluconic acid 18

1.6.2 Synthesis of Gluconic acid 19

1.6.3 Glucaric acid 20

1.6.4 Synthesis of Glucaric acid 22

1.7 Electrocatalysis 23

1.7.1 Hydrolysis of water and Oxygen evolution 25

1.7.2 Electrocatalytic oxidation 27

1.7.3 Electrocatalytic oxidation of glucose for sensors 28

1.8 Selective oxidation of glucose to gluconic and glucaric acid 31

1.9 Electrocatalyst with high surface area 33

1.9.1 Deposition methods 34

2. Experimental part 37

2.1 Material and reagents 37

2.2 Electrocatalysts preparation 37

2.3 Characterization techniques....38
2.3.1 SEM....38
2.3.2 Raman Spectroscopy....40
2.3.3 X-ray Diffraction....41
2.4 Electrochemical test....42
2.5 Analysis of reaction products....44
2.5.1 High-performance liquid chromatography (HPLC)....44
3. Results and discussion....47
3.1 Characterization of the metal foams....47
3.2 Electrochemical characterization of foams: cyclic voltammetry in NaOH and Glucose 10mM and 50mM....52
3.3 Electrochemical oxidation of glucose....58
3.3.1 Catalytic test in a solution of glucose 10mM....59
3.3.2 Cyclic voltammetry after catalytic tests....61
3.4 Effect of the charge on electroactivity....64
3.5 Effect of glucose concentration....65
3.5.1 Electrochemical tests with 50 mM glucose solution....65
3.5.2 Electrochemical tests with 100mM glucose solution....68
3.6 Characterization after reaction....71
Conclusions....73
Bibliography....75

Aim of the work

Nowadays one of the most important scientific and environmental concern is to reduce global dependence on fossil fuels.

Among the possible viable routes, the use of lignocellulosic biomass makes it possible to obtain important platform molecules such as D-glucose, from whose selective oxidation it is possible to synthesize high added-value chemical products such as gluconic acid (GO) and glucaric acid (GA).

These two products lend themselves to a wide range of applications, including the production of high commercial potential compounds such as adipic acid, a nylon precursor, currently derived from fossil sources and with thermo catalytic processes.

An alternative to the thermochemical process is the electrocatalytic pathway that in recent years has been gaining considerable interest. Electrocatalytic processes allow the use of ambient temperature and pressure and of green solvents such as water. Furthermore, the possibility of carrying out the entire process with electricity produced from renewable sources makes it completely sustainable.

At present the studies on the electro-oxidation of D-glucose are particularly focused on its use in medical devices for the detection of D-glucose in the human blood, trying to exploit its electrochemical oxidation to obtain gluconic acid and glucaric acid. In a previous work of the research group it was shown that Ni is a promising material to synthesize selective electrocatalysts for D-glucose electro-oxidation.

In this context, the aim of the present thesis work was to further investigate Ni materials as electrocatalysts for the D-glucose electrooxidation, also studying the role of the potential applied and of D-glucose concentration on the selectivity and faradic efficiency.

Electrocatalysts based on open-cell Ni metal foams were investigated for the glucose electrooxidation. They were used as supplied, oxidized at 500°C and 600°C, and after electrodeposition of $Ni(OH)_2$. The electrocatalysts were characterized by cyclic voltammetry in NaOH solution 0.1M and in a basic D-glucose solution with different glucose concentrations (10mM and 50mM). The effects of the potential applied, the glucose concentration and the reaction time on conversion, selectivity and faradic efficiency were also investigated.

3D Ni electrocatalyst showed promising activity in the conversion of glucose towards gluconic acid, the sample calcined at 500°C provided the best results.

1. Introduction

The use of renewable sources is becoming increasingly necessary as a substitute of fossil raw materials in the production of energy, fuels and chemicals. It is well known that the use of fossil fuels represents by far the largest source of emissions of greenhouse gasses (GHG). Within the energy sector, CO_2 deriving from fuel combustion dominates total GHG emissions, resulting as the determining factor of the global warming: in the 2018 annual review, of the International Energy Agency (IEA) it was reported that the amount of emitted CO_2 was over 33Gt. [1]

Another remarkable reason is the velocity at which these resources are consumed. Global fossil fuel consumption is on the rise and new reserves are becoming harder to find. It is estimated that all the known oil deposits could run out in 53 years, gas reserves in 52 years, and coal deposits in 150 years. [2]

In this context it is important to move towards a sustainable development that meets the needs of the present without compromising the ability of future generations to meet their own needs.

One strategy of the chemistry's sustainable development could be the employment of biobased raw materials that allow a decrease in the use of fossil-based material and a decrease of CO_2 emission. It is fundamental, than, to decrease the dependency on this materials through the research of new technologies in common with the optimization of systems that could be able to produce energy and materials from renewables and to protect the environment. [3]

It is defined as renewable a source of energy or material that do not deplete or can be powered within a human's lifetime. The most common examples include wind, sunlight, geothermal, biomass and hydropower.

In particular, the biomass is becoming nowadays an economic and sustainable important topic especially for its use and transformation to produce energy and chemicals.

1.1 Biomass

Biomass is defined as the biodegradable fraction of products, waste and residues from agriculture (including vegetal and animal substances), forestry and related industries including fisheries and aquaculture, as well as the biodegradable fraction of industrial and municipal waste [4].

Biomass is the most common form of renewable energy, widely used in the third World but, until recently, less in the Western world. Biomass is the plant material derived from the reaction between CO_2 in the air, water and sunlight, via photosynthesis, that produces carbohydrates that form the building blocks of biomass (Fig 1.1). Biomass is processed efficiently, either chemically or biologically, by extracting the energy stored in the chemical bonds and oxidising the carbon to produce CO_2 and water. The process is cyclical, as the CO_2 is then available to produce new biomass [5].

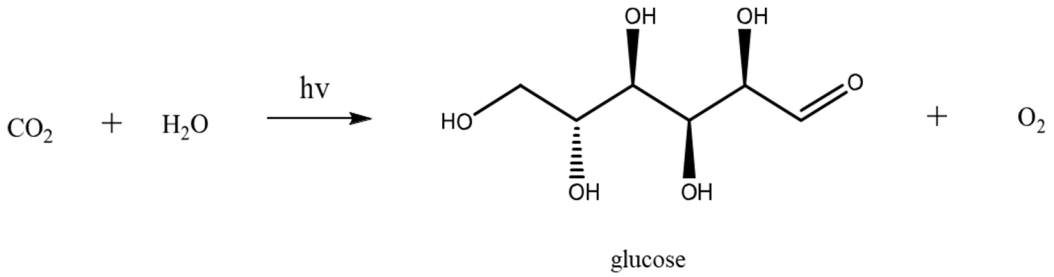

Figure 1.1: photosynthesis overall reaction

The photosynthesis is not an ideal process since the solar energy is not efficiently converted into chemical energy. From the energy held in the incident solar radiation only the 0,15-0,50% is converted [6].

In spite of the low conversion efficiency, the different functionalities present on the monomers of the biomass allow to convert them into most of the materials that are usually obtained from fossil feedstocks; this could simplify the chemical production processes, limiting the amount of side-products and wastes, in agreement with some of the green chemistry principles [7] [8].

One simple way to classify the various types of biomass is to define three main types, accordingly to their origin:

- First generation: from dedicated crops taken away from the agri-food industry, therefore in competition with it. They are usually obtained from sugar, starch, vegetable, animal or vegetable fats, corn and wheat.
- Second generation: from non-food agriculture, lignocellulosic materials such as agriculture or processing wastes.
- Third generation: from aquatic environment such as seaweeds.

Looking at this list, it is easily recognisable that the second and third generation biomass match well with the economical and sustainable concept to follow for a better future, allowing the production of new resources from the re-use of wastes.

1.1.1 Lignocellulosic biomass

Lignocellulosic biomass is the most abundant biomass on earth, and it holds enormous potential for sustainable production of chemicals and fuels.

Lignocellulosic biomass is mainly composed of three polymers: cellulose, hemicellulose and lignin together with small amounts of other components like acetyl groups, minerals and phenolic substituents (Fig. 1.2) [9].

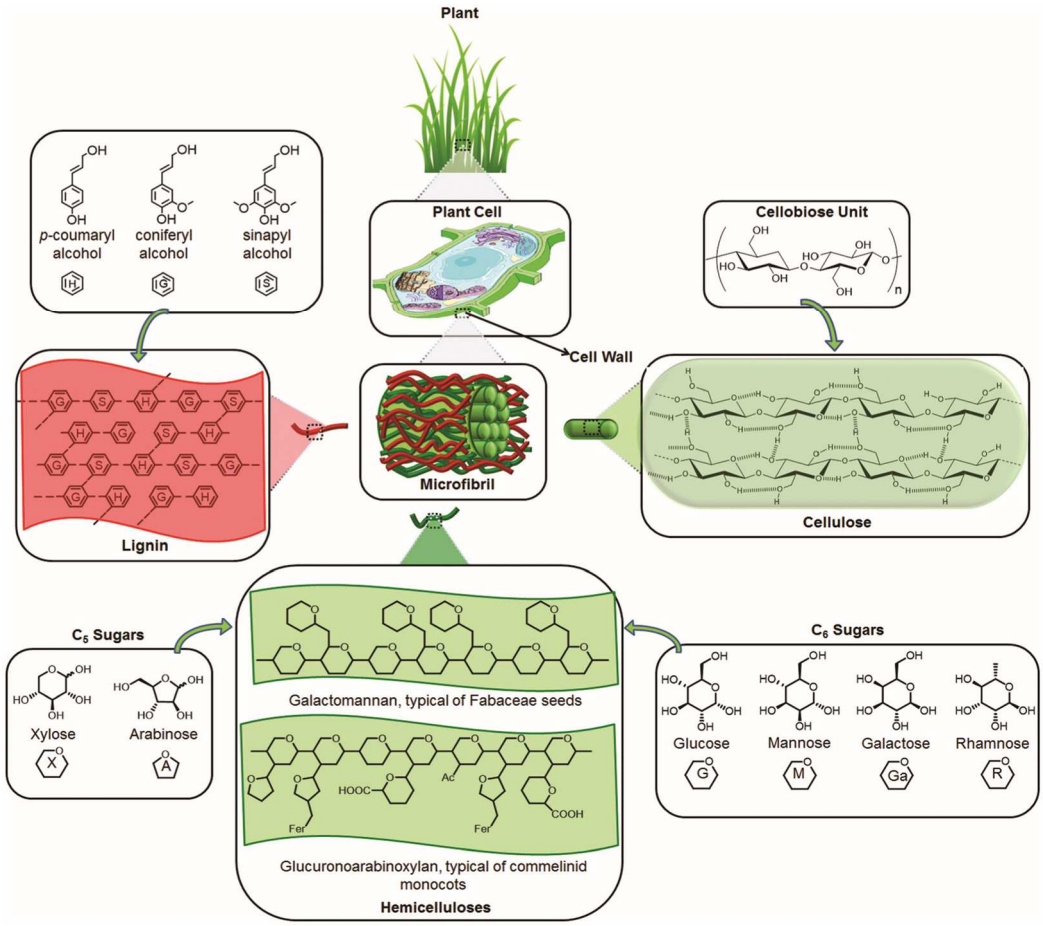

Figure 1.2: main components and structure of lignocellulose

The major component of lignocellulosic biomass is cellulose, about 40-50%. It is the strongest potential candidate for the substitution of petroleum-based polymers owing to its eco-friendly properties like renewability, biocompatibility and biodegradability.

The structure of cellulose consists of extensive intramolecular and intermolecular hydrogen bonding networks, β(1,4)-glycosidic bonds, which tightly bind the D-glucose units to form a linear polymer chain.

The cellulose is insoluble in water and most organic solvents, the hydroxyl groups form hydrogen bonds with oxygen atoms on the same or on a neighbour chain, holding the chain firmly together side-by-side and forming microfibrils with high tensile strength [10]. The mechanical role of cellulose fibers in the wood matrix is responsible for its strong structural resistance.

The second most abundant polymer, 20-30%, is the hemicellulose. Unlike the cellulose it has a random and amorphous structure which is composed by several heteropolymer

including xylan, galactomannan, glucuronoxylan, arabinoxylan, glucomannan and xyloglucan (Fig1.2).

Hemicelluloses are imbedded in the plant cell walls to form a complex network of bonds that provide structural strength by linking cellulose fibres into microfibrils and cross-linking with lignin.

It is easily hydrolysable due to the absence of crystal domain; there are different types of hemicellulose but the most common composition is composed by xylanic β (1,4)-glycosidic units, where 20% of monomers present ramification [11].

The third component is lignin, about 10-25%, a three-dimensional polymer of phenylpropanoid units. It functions as the cellular glue which provides compressive strength to the plant tissue and the individual fibres, stiffness to the cell wall and resistance against insects and pathogens.

The oxidative coupling of three different phenylpropane building blocks (monolignols): p-coumaryl alcohol, coniferyl alcohol and sinapyl alcohol, forms the structure of lignin [9].

Proteins, oils, ash, inorganic salts of Si, K, Na, S, Cl, P, Ca, Mg and Fe make up the remaining fraction.

1.2 Biorefinery

This century faces environmental problems, a food crisis and the challenge of the coming "cosmic era". The technologies to address these issues are interrelated, and the biorefinery is one of them, allowing an efficient use of the raw materials to produce fuels, solvents, plastics and food for human beings with the so called "zero waste" philosophy (Fig. 1.3).

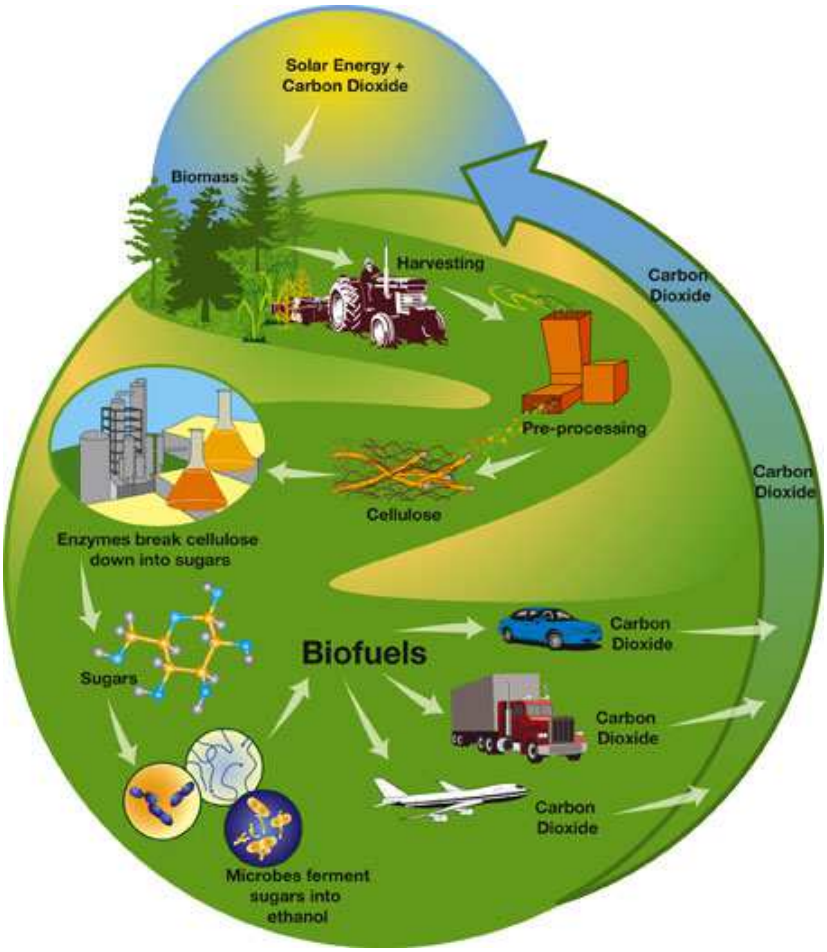

Figure 1.3: biofuel cycle in the biomass treatment *[12]*

The biorefinery mediates between environment and society and has positive economic impacts. It can be classified into two types: biomass-producing-country type and waste-material-utilization type; in countries such as Brazil, the United States, China, Southeast Asia and Australia, biomass such as sugarcane, corn, sugar beet, cassava, sago and potatoes are used in biorefineries. These countries are going to breath-life into a new industry, using agricultural products. Japan and some European countries do not have enough space for garbage landfill, have insufficient field for compost and have few agricultural products. In these countries refuse disposal and environmental pollution policies are connected and the biorefinery serves the dual role of refuse disposal and production of useful products. Old paper, lumber waste, animal waste and food waste provide the raw material for fermentation and energy resources [13].

The main problem due to the utilization of the biomass comes from the relatively high treatment costs associated to the new and not optimized processes; from the low energy

density, equal to half of the fossil fuels and from the biomass supply, different based on the agricultural season that makes necessary its controlled storage.

Furthermore, compared to fossil fuels, the biomass is composed by a lower percentage of Carbon and Hydrogen while the Oxygen, Sulphur and Nitrogen are usually present in a higher amount.

Despite these problems, the great energetical and chemical potential of the biomass make the use of this source suitable thanks to the high added value of the final products (Fig. 1.4).

Bio-PM	Structure	Bio-PM	Structure
glycerol	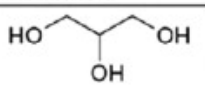	(S, R, R)-xylitol	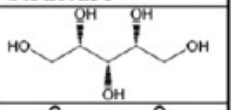
3-hydroxy propionic acid	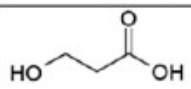	L-glutamic acid	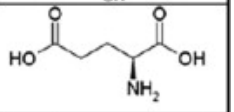
L-aspartic acid	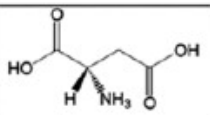	itaconic acid	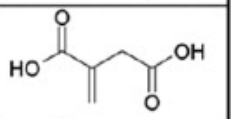
fumaric acid	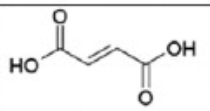	levulinic acid	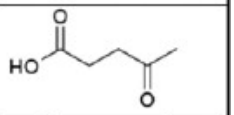
3-hydroxy butyrolactone	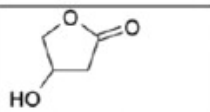	2,5-furan-di-carboxylic acid	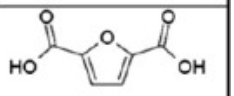
L-malic acid	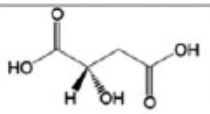	glucaric acid	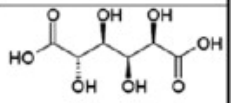
succinic acid	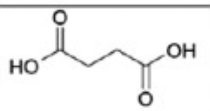	sorbitol	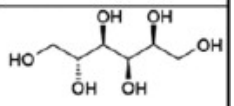

Figure 1.4: platform molecules derived from biomass *[14]*

While cellulose and hemicellulose are polysaccharides that can be hydrolysed to sugars and then fermented to ethanol, lignin cannot be used in fermentation processes. Furthermore, due to very intricate hydrogen bonding such as intra-, inter-molecular and inter-sheet in cellulose and multiple bonding between polysaccharides and lignin, it becomes complicated to process lignocelluloses directly into sugars. During the conversion of the polysaccharide part (cellulose and hemicellulose), lignin remains unconverted because it usually requires high processing temperatures (>250°C)

compared to polysaccharides (<230°C). Moreover, if conversions of lignin are also tried simultaneously then degradation reactions of sugars become predominant. In most cases, unconverted lignin is also capable of poisoning the catalytically active sites.
Hence, it becomes indispensable to pre-treat the lignocelluloses before hydrolysis for the removal of lignin and decrease of the cellulose crystallinity. During some of the pre-treatments, the degree of polymerization (DP) of cellulose decreases, which may increase the solubility of cellulose (fractions) in water for efficient hydrolysis [15].

1.3 Lignocellulosic biomass pre-treatment

The available biomass pre-treatment methods are classified roughly into three categories namely: (1) physical (milling, grinding, radiation, ultrasound), (2) physico–chemical (steam explosion, ammonia fiber explosion, carbon dioxide explosion) and (3) chemical (ozonolysis, alkaline hydrolysis, oxidative delignification, organic solvent extraction, acid hydrolysis, enzyme treatment, and ionic liquid treatment) [16].

1.3.1 Physical Treatment

The main purpose of the physical pre-treatment of lignocellulose is to decrease its particle size and cellulose crystallinity. Use of milling and grinding methods can decrease the size of various biomass to 0.2–2 mm from 10– 30 mm [17].
During ball milling an increase in temperature is observable, which influences de-crystallization; for this reason it becomes important to control the temperatures for reproducible results. Recently, an ultrasound technique has been used to decrease cellulose crystallinity within a short time in the presence of water. It is assumed that when cellulose is exposed to ultrasound, the H-bonding is broken to form lower crystallinity cellulose [18].
Other innovative methods used as physical treatment are: 1) microwave irradiation, which causes localized heating of lignocellulose, leading to disruption of the lignocellulose structure [19]; 2) γ-rays irradiation, leading to the reduction of DP and crystallinity in cellulose [20].
However, in terms of cost and generation of high temperature during treatment, these processes are not efficient on a large scale.

1.3.2 Physico-Chemical Treatment

There are many physico-chemical treatments, the most common are:

Steam explosion: the biomass is treated with saturated steam (6.9–48.3 bar) at high temperatures (160–260 °C) and after a certain time (few seconds to a few minutes) the pressure is suddenly reduced to atmospheric pressure, bringing the biomass to undergo an explosive decompression. This process helps in the removal of hemicellulose and redistribution of lignin. Moreover, the addition of mineral acid (H_2SO_4/CO_2 = 0.3–3 wt/wt) during steam explosion, improves the efficiency of the pre-treatment process by decreasing the temperature and time required.

The steam explosion treatment has advantages including a lower energy requirement than mechanical treatment (70% less energy requirement) and less environmental impact, which allows the process to operate on an industrial scale successfully [21].

The main problems are the acid degradation of sugars with subsequentially formation of side-products, as aldehydes, which must be separated. Moreover, a washing in water is needed in order to eliminate inhibitor compounds for possible microbiological treatments.

Liquid hot water (LHW): the pretreatment uses water at high temperatures and pressures to maintain its liquid form in order to promote disintegration and separation of the lignocellulosic matrix. Temperatures can range from 160°C to 240°C and over time periods ranging from a few minutes up to an hour. Temperature determines the types of sugar formed and time determines the amount of sugar; for example, 180°C (low end of temperature range) and 30 minutes (moderate-high time-scale range) have seen to be the most cost-effective pretreatment condition for rice straw conversion to glucose [22].

The generation of reactive cellulose fibers to produce pentosans as well as disruption of the entire lignocellulosic matrix is achieved through the cell penetration of the biomass by the water; at the same time the solubilisation of both hemicellulose and lignin takes place thanks to the hot liquid water that acts like an acid [23].

This process can be seen as advantageous from a cost standpoint in that no additives such as acid catalysts are required; furthermore, expensive reactor systems are not necessary thanks to the low corrosive nature of this pretreatment technique and the chemicals that are involved.

Ammonia fiber explosion (AFEX): the biomass material is subjected to liquid anhydrous ammonia under high pressures and moderate temperatures (60°C to 100°C) and is then rapidly depressurized. The temperatures are significantly less than that of the steam explosion process, meaning less energy input and overall costs associated with the process.

The degree of disruption to the biomass structure will depend on the temperature, as it will affect the rapidness of the ammonia vaporization within the reactor during depressurization. This rapid expansion of the ammonia gas causes swelling of the biomass feedstock, creating a disruption in the lignin-carbohydrate linkage, hemicellulose hydrolysis, ammonolysis of glucuronic cross-linked bonds and partial decrystallization of the cellulose structure; all leading to a higher accessible surface area for enzymatic attack [24] [25].

As advantages this process products a low moisture content, low formation of sugar degradation products, 100% recovery of solid material; but it needs the recovery of the ammonia gas in order to reduce the operating costs of the pretreatment.

Ammonia recycle percolation (ARP): in this process, aqueous ammonia with concentration between 5–15% (wt%), is sent through a packed bed reactor containing the biomass feed stock at a rate of about 5 mL/min. Moderately high temperatures (140°C to 210°C) and longer reactions times are used in comparison to the AFEX process, creating higher energy costs [26].

The advantage of this process over AFEX is its ability to remove most of the lignin (75–85%) and solubilise more than half of the hemicellulose (50–60%), while maintaining a high cellulose content [27]. This is due to the selectivity of ammonia and its ability to break down lignin by ammonolysis, while also solubilising hemicellulose over the longer retention times.

High energy costs and liquid loadings, along with many disadvantages associated with the AFEX process, are still some major concerns that need to be addressed before this process is proven to be economical [25].

Supercritical fluid (SCF) pretreatment: a supercritical fluid shows unique properties that are different from those of either gases or liquids under standard conditions. It possesses a liquid-like density and exhibits gas-like transport properties of diffusivity and viscosity. Thus, SCF has the ability to penetrate the crystalline structure of lignocellulosic biomass overcoming the mass transfer limitations encountered in other pretreatments [28].

Supercritical carbon dioxide (CO_2) with a critical temperature (T_c) of 31°C and a critical pressure (P_c) of 7.4 MPa, has excellent potential for biomass pretreatment. When used in combination with water, it forms carbonic acid which favours polymer hydrolysis. Once the biomass is pretreated, explosive release of CO2 disrupts the cellulose and hemicellulose structure, thus increasing the accessible surface area for enzyme hydrolysis.

The lower temperatures used in the process helps for the stability of the sugars and prevents degradation observed in other pretreatments.

Even though SCF is being investigated by several researchers for pretreatment, the whole process has not proven to be economically viable due to the high pressures involved. Improvements need to do to implement the process on a large scale [25].

1.3.3 Chemical Pretreatments

There are several chemical processes and they are the most studied due to their simplicity.

Alkaline pretreatment: involves the use of bases, such as sodium, calcium and ammonium hydroxide, for the pretreatment of lignocellulosic biomass. The use of alkali causes the degradation of ester and glycosidic side chains resulting in structural alteration of lignin, cellulose swelling, partial decrystallization of cellulose and partial solvation of hemicellulose [29] [30].

The conditions for alkaline pretreatment are usually less severe than those for other pretreatments. It can be performed at ambient conditions, but longer pretreatment times are required than at higher temperatures.

Acid pretreatment: involves the use of concentrated and diluted acids to break the rigid structure of the lignocellulosic material. The most commonly used acid is dilute sulphuric acid (H_2SO_4), which has been commercially used to pretreat a wide variety of biomass types; other acids have also been studied, such as hydrochloric acid (HCl) [31], phosphoric acid (H_3PO_4) [32], and nitric acid (HNO_3) [33]. Due to its ability to remove hemicellulose, acid pretreatments have been used as parts of overall processes in fractionating the components of lignocellulosic biomass [32]. Acid pretreatment (removal of hemicellulose) followed by alkali pretreatment (removal of lignin) results in relatively pure cellulose.

A key advantage of acid pretreatment is that a subsequent enzymatic hydrolysis step is sometimes not required, as the acid itself hydrolyses the biomass to yield fermentable sugars. However, due to the corrosive nature and toxicity of most acids, an adequate material for the reactor is required in order to withstand the required experimental conditions and corrosiveness of the acids [25].

Wet oxidation: utilizes oxygen as an oxidizer for compounds dissolved in water. There are two reactions that occur during this process. One is a low temperature hydrolysis reaction and the other is a high temperature oxidation reaction [34].

A compound, usually Na_2CO_3, is introduced to the mixture to reduce the formation of byproducts. Air is pumped into the vessel until a pressure of 12 bar is reached. This method of pretreatment is performed at 195°C for a range of 10 to 20 minutes. Wet oxidation can be used to fractionate lignocellulosic material by solubilizing hemicellulose and removing lignin; during wet oxidation lignin is decomposed to carbon dioxide, water, and carboxylic acids [35]. The amount of lignin removed after pretreatment ranges from 50% to 70%, depending on type of biomass pretreated and the conditions used.

Green solvents: uses ionic liquids (IL) and other solvents, the process, has gained importance in the last decade, due to the tunability of the solvent chemistry and hence the ability to dissolve a wide variety of biomass types.

The low vapor pressure of IL and similar solvents make them more than 99% recoverable in several operations, thus reducing costs of solvent usage. Since no toxic products are formed during the pretreatment operation and IL are recoverable, they are termed green solvents [36].

The anion of the IL forms hydrogen bonds with cellulose (sugar hydroxyl protons) in a 1:1 ratio and breaks up the cellulose crystalline hydrogen bonded structure, thus making it more amorphous and accessible to enzymatic hydrolysis. In addition, the chemistry of the IL can also be tuned to dissolve the hemicellulose and lignin, thus making it suitable to dissolve the different components. It should be mentioned here that the IL dissolves cellulose and generally does not degrade the chains and reduce its degree of polymerization [25]

1.4 Hydrolytic processes for the glucose production

In order to utilize cellulose as a feedstock for production of chemicals, its conversion to glucose is essential and it is accomplished by hydrolytic processes catalysed by an enzyme or an acid (Fig. 1.5).

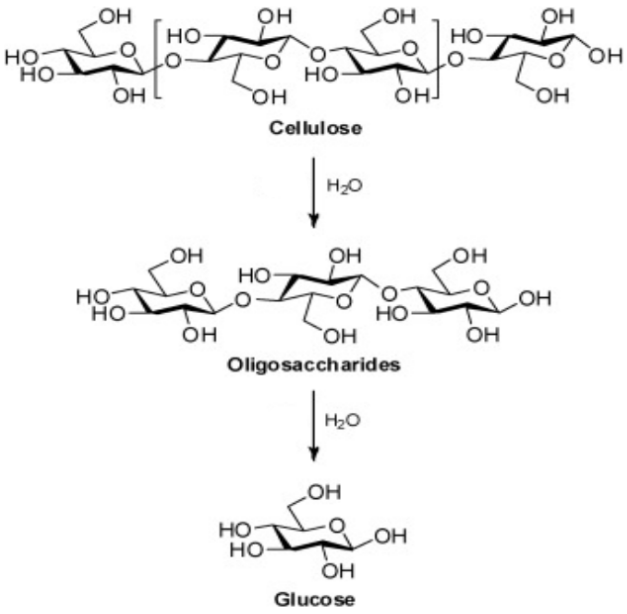

Figure 1.5: cellulose hydrolysis

When cellulase enzyme systems act in vitro on insoluble cellulosic substrates, three processes occur simultaneously: 1) chemical and physical changes in the residual (not yet solubilized) solid-phase cellulose; 2) primary hydrolysis, involving the release of soluble intermediates from the surface of reacting cellulose molecules; 3) secondary hydrolysis, involving hydrolysis of soluble intermediates to lower molecular weight intermediates and ultimately to glucose. Endoglucanase increases the concentration of chain ends and significantly decreases DP by attacking interior portions of cellulose molecules. Exoglucanase attacks the ends of the chains and frees cellobiose as main product; at the end β-glucosidase hydrolyses cellobiose to glucose. [37].

The other method involved in the cellulose hydrolysis regards the use of mineral acids as HCl, H_2SO_4 e H_3PO_4. Nowadays the researchers are studying the effect of solid acid

catalysts as the heteropolyacids, polyvalent metal salts and sulfonic acids supported on mesoporous silica or active carbons; the use of heterogeneous catalysts allows to a better separation of products but the amount of catalyst needed still remain the major drawback for this application [38].

Enzymatic hydrolysis has several advantages over acid hydrolysis: the enzymes hydrolysing cellulose are very specific and do not produce undesirable by-products; at the end of the hydrolysis the neutralization of the product is not required; capital and operating cost are substantially lower since enzymatic hydrolysis takes place at mild temperatures and expensive corrosion-proof equipment is not required.

The advantages of acid hydrolysis include short reaction time and the ability to utilize cellulose without expensive pretreatment [39].

1.5 Glucose and its derivatives

Glucose is a monosaccharide containing six carbon atoms and an aldehyde group and is therefore referred to as an aldohexose. The glucose molecule can exist in an open-chain (acyclic) and ring (cyclic) form (Fig. 1.6).

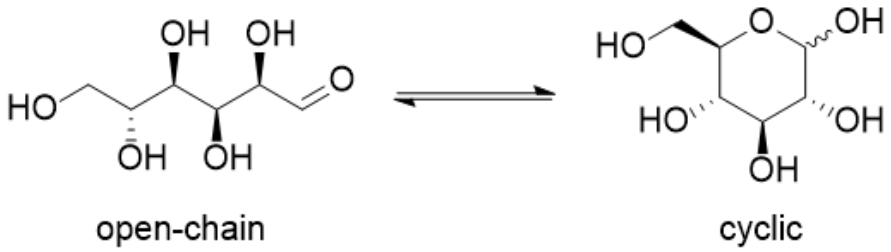

Figure 1.6: Open-chain and pyranose forms of glucose

In water solution both forms are in equilibrium and at pH 7 the cyclic one is the predominant, being the result of an intramolecular reaction between the aldehyde C atom and the C-5 hydroxyl group to form an intramolecular hemiacetal.

This reaction is reversible and bring to the existence of two cyclic enantiomeric structures termed α and β anomer, distinguishable from the hemiacetal OH group position on C-1 (Fig. 1.7). The glucose has a low reactivity toward the reactions that involve the aldehydes due the small percentage, around the 0,0026%, of the open chain form at pH equal to 7 respect to the cyclic one. Increasing the pH the β enantiomer is

favoured respect to the α one and at pH equal to 13 the ratio α:β is 22:78 (0,1 M di NaOH) [40].

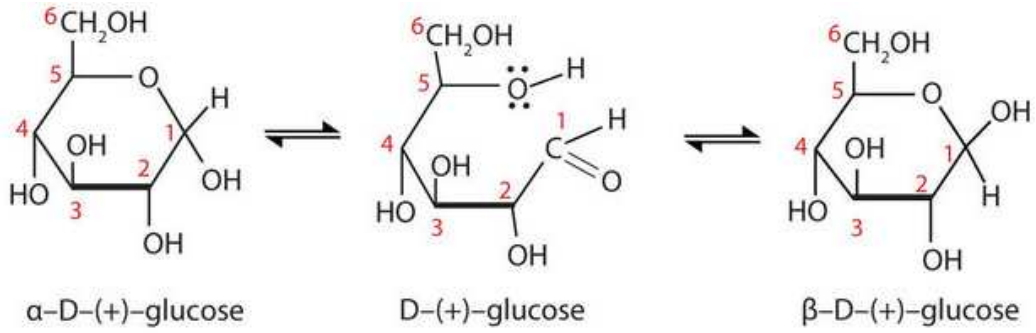

Figure 1.7: α and β anomer of glucose in water

At high pH values the glucose is involved in reversible isomerization reactions that give rise to an equilibrium with fructose and mannose through a rearrangement of enediol intermediates (Fig. 1.8). In base condition, the glucose has a very strong reductant ability that can promote reaction as: self-oxidation, interconversion, polymerization and so on, giving rise, after a long exposure, to the formation of 116 different products [41].

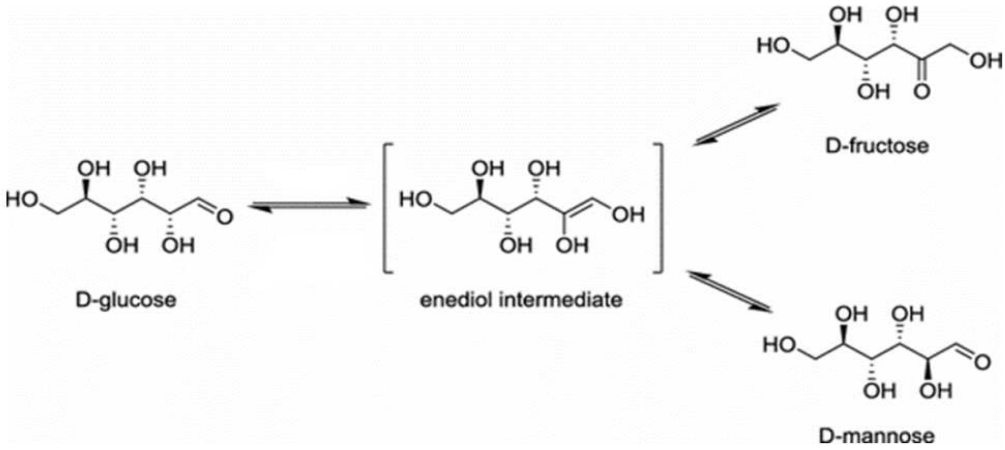

Figure 1.8: equilibrium between glucose and its isomers in alkali media

Due the intrinsic chirality of the glucose, two enantiomeric forms exist, L and D (Fig. 1.9), and the latter is the form of Glucose that is found abundant in nature. It is the basic form of energy storage and living beings use D-Glucose to fulfil their energy needs.

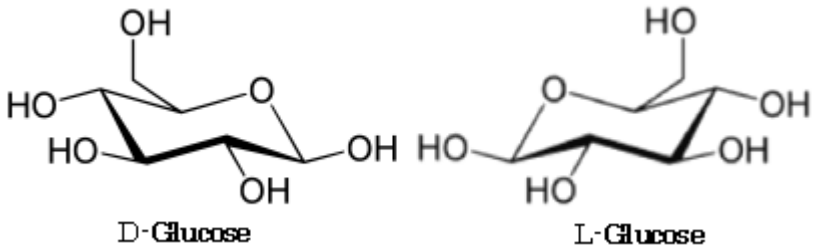

Figure 1.9: enantiomeric forms of glucose

Due to the different processes in which the glucose can be involved, many platform molecules can be obtained as the 5-hydroxymethylfurfural (HMF) and the levulinic acid (fig. 1.10).

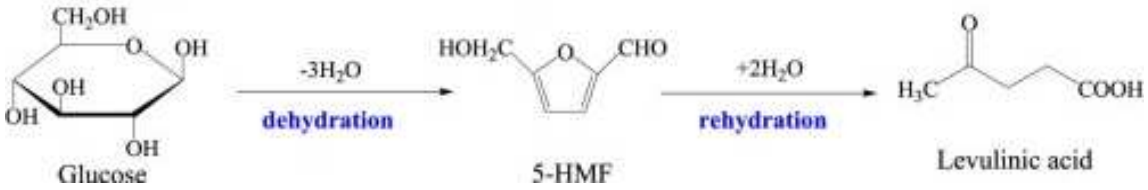

Figure 1.10: platform molecules obtained from the glucose

Moreover, oxidising the glucose is it possible to obtain mono and poly carboxylic acid as the gluconic acid (GO) and the glucaric acid (GA) (Fig. 1.11), objects of interest of this thesis.

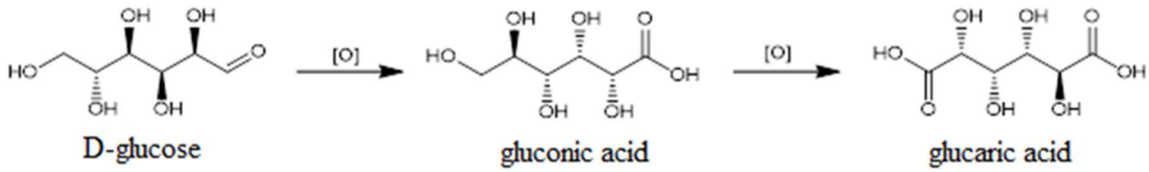

Figure 1.11: oxidation od D-glucose to gluconi and glucaric acid

1.6 Oxidation products of the glucose

In oxidation reactions depending on which part of the molecule of glucose reacts many products can be obtained; it is possible to gather these molecules in three main groups depending on the glucose functional group involved in the reaction.

- **Aldaric acids** (previously called saccharic acids) are polyhydroxy dicarboxylic acids, $HO_2C(CHOH)_nCO_2H$, that are formally produced by oxidation of aldoses at both termini; they are primarily obtained from sugars, aldonic acids, and oligo- or polysaccharides by reaction with strong oxidizing agents.

End-to-end symmetry allows internal compensation, so that various meso (optically inactive) forms exist and different aldoses may form identical aldaric acids. For instance, d-glucose and l-gulose give the same product: d-glucaric acid=l-gularic acid (Fig. 1.12).

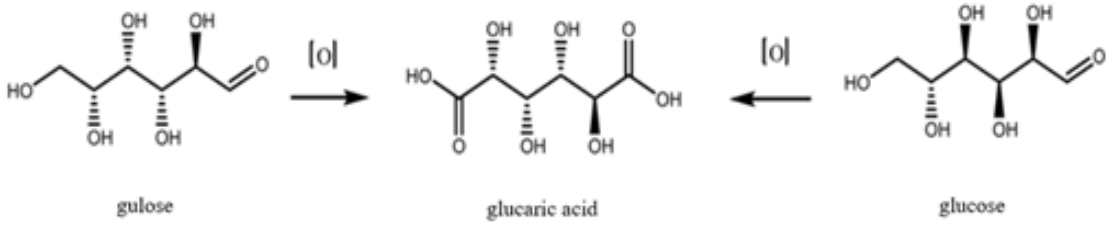

Figure 1.12: different ways for glucaric acid synthesis

Glucaric, citric, tartaric and succinic acids are the most industrially employed polycarboxylic acids; for example, the citric and the tartaric acid are commonly used in food industry, while the succinic acid is mostly utilized in industry such as for the synthesis of polyester, polyamide.

- **Aldonic acids** are polyhydroxyacids derived from an aldose through the partial oxidation of the aldehydic group. Br_2 is commonly employed as oxidising agent. Aqueous solutions of aldonic acids undergo equilibration between the acid and lactone forms if this is not prevented by substitution; the proportion of acid and lactone depends on the configuration of the asymmetric carbon atoms.

  The industrially most synthetize compound is the gluconic acid used for the glucaric acid production.
- **Uronic acids** may be regarded as aldoses in which the primary alcoholic group has been oxidized to a carboxyl group or, alternatively, as aldos-ω-onic acids. As with aldoses, they can exist in both furanose and pyranose forms and, like aldonic acids, they can lactonize.

  The uronic acids occur naturally in combined form, mainly as constituents of polysaccharides. D-glucuronic acid (Fig. 1.13) is also present in metabolic products of low molecular weight [42].

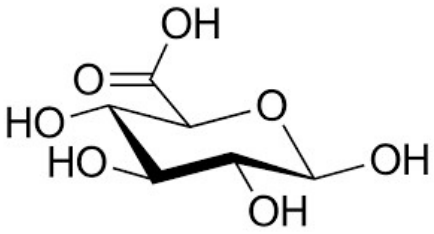

Figure 1.13: D-glucuronic acid

1.6.1 Gluconic acid

Gluconic acid, or pentahydroxycaproic acid (C6H12O7), naturally occurs in plants, fruits, wine, honey, rice, meat, vinegar, and other sources. The alkali salt of gluconic acid such as calcium gluconate or sodium gluconate has multiple applications in chemical, pharmaceutical, food, beverage, and construction industries [43].

Because it is both an acid and an alcohol, GO can undergo 1,5 intramolecular esterification. The process is favoured by an acidic medium and involves the spontaneous loss of a water molecule to yield intramolecular anhydride glucono-δ-lactone, which is a cyclic ester. In aqueous solutions, the acid is in equilibrium with its lactone (Fig. 1.14) [44].

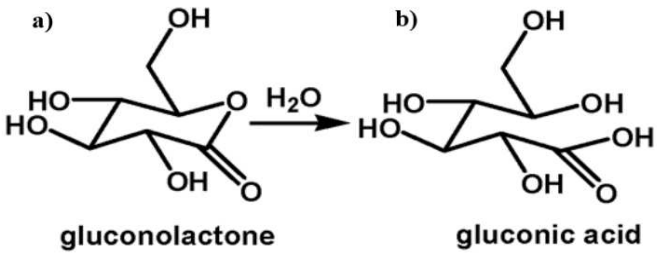

Figure 1.14: equilibrium between a) glucono-δ-lactone and b) gluconic acid

Adding a base to the ester it rapidly cleaves the aldonic ring to yield an open chain salt: a gluconate. This salt can easily bind di-and trivalent metals to form highly stable chemical compounds, that can only react with strong oxidants such as nitric acid or hydrogen peroxide.

Due to its low toxicity, low corrosiveness and high capability of forming water-soluble complexes with divalent and trivalent metal ions, sodium gluconate has been designated

as GRAS (Generally Recognized As Safe) by the US FDA (Food and Drug Administration). This acid is also recognized as a generally permitted food additive (E574) by European Parliament and by Council Directive No. 95/2/EC [45]. Like other organic acids, gluconic acid has diverse uses that range widely depending on their particular structure.

Furthermore, the excellent chelating properties of GO with Fe^{2+} and Fe^{3+} have been used to remove, at neutral pH, hazardous chlorinated substances such as 2,4,6-trichlorophenol (TCP) and trichloroethylene from ground water through the Fenton reaction [46].

1.6.2 Synthesis of Gluconic acid

There are five different processes for the synthesis of the gluconic acid: 1) chemical oxidation of the glucose with halides as oxidising agents [47] [48]; 2) electrolytical oxidation of a glucose solution with bromide; 3) biotechnological processes of fermentation [49] and 4) enzymatic processes [47] [50] 5) catalytic processes [51] [52].

In the glucose oxidation process via heterogeneous catalysis in an aqueous solution, the efficiency of the process depends on the activity, selectivity and stability of the catalyst. Most research in this area has focused on catalysts of noble metals (Pd, Pt and Au) supported on TiO_2, Al_2O_3 or activated carbon, among other solids. In fact, supported Au nanoparticle (NPs) show both high selectivity and high stability, an example is the easy oxidation of the aldehyde group of D-glucose to give GO in slightly alkaline conditions (pH range 8-10, necessary to neutralize the acid produced) or even in the absence of a base and keep the surface of the catalyst clean. A variety of Au-based catalysts are reported in the literature (Au / MgO, Au / CeO_2, Au / Al_2O_3 and Au / TiO_2) and they have shown optimal performance, with GO yields higher than 80%. For catalytic oxidation, alkaline solutions are generally used at temperatures between 20 °C and 80 °C with pH between 8-11, which increases the reaction rate and avoids the rapid deactivation of the catalyst [51] [52], kept constant by the continuous addition of the alkali metal hydroxide which will form the final gluconate.

The yield of GO, then, is a function of the reaction conditions (pH, temperature, pressure O_2) and of the method used for the preparation and deposition of the NP.

Although doping with Bi has been found to increase the catalytic activity, the poor stability of the resulting catalysts against leaching has hindered the use of synthetic

gluconate for nutritional and pharmaceutical purposes [52]. Gold-based catalysts are excellent choices for glucose conversion into GA [53]; however, the decline in activity after the second catalytic cycle has hindered their implementation at the industrial scale [52].

1.6.3 Glucaric acid

D-Glucaric acid, also called saccharic acid, is a chemical compound with formula $C_6H_{10}O_8$ (Fig. 1.15) and member of a large family of molecules known as oxidized sugars. It is a naturally occurring aldaric acid, typically found in small amounts in a variety of fruits and vegetables.

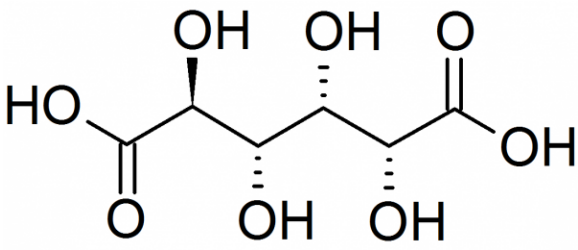

Figure 1.15: D-Glucaric acid

Being a highly functionalized compound with four chiral carbons and many reaction pathways, its commercial potential was unveiled in the report "Top Value Added Chemicals from Biomass" from the Department of Energy of USA which described its use as a building block for a number of polymers, including new nylons and hyperbranched polyesters [9] [54](Fig. 1.16).

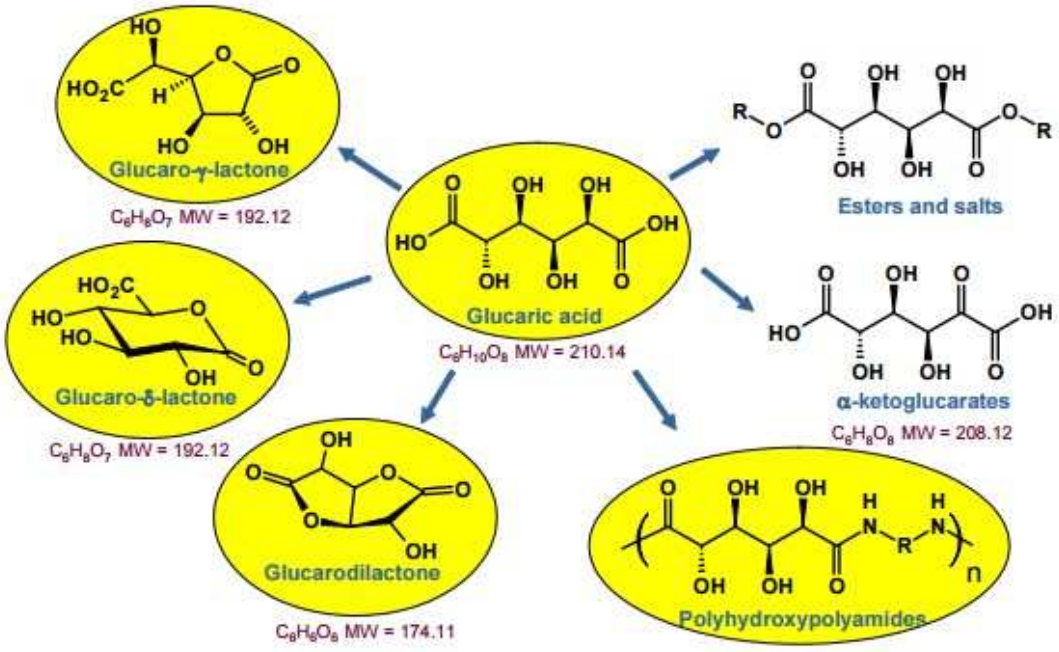

Figure 1.16: Derivatives of glucaric acid

The glucaric acid has many applications, one of the most used is as an intermediate for the adipic acid (Fig. 1.17) production from renewable sources [55] [56].

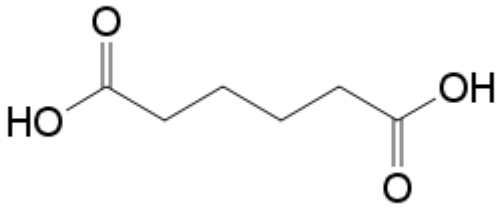

Figure 1.17: structure of the adipic acid

Adipic acid ($(CH_2)_4(COOH)_2$) is considered as an important bulk chemical and is a precursor for the production of nylon-6,6. About 80% of the world-wide adipic acid production is used for the production of this polymer.

Other applications of glucaric acid:

- Phosphate-free detergents and biodegradable cleaners. The salts of sugar acids can be applied to chelate various metal ions. Those detergent builders demonstrate binding capacity to sequester free calcium at a rate comparable to that of phosphates.

- Anti-corrosion additives. Glucaric acid has the capacity to drop pH in operating conditions to levels suitable for various applications in upstream and downstream oil and gas development [57].
- Cement and concrete additives [58].
- Adhesives and coatings.
- Food ingredients and animal feed acidulant.
- Therapeutic. Antitumor agent via inhibition of carcinogen-DNA binding and cholesterol-reducing agent [59].

1.6.4 Synthesis of Glucaric acid

The synthetic preparation of D-glucaric acid dates back to a report of Sohst and Tollens (1888) who carried out the nitric acid oxidation of D-glucose to D-glucaric acid. Current methods for its production are based on this process and involve the chemical oxidation of D-glucose, frequently with nitric acid [60] [61]. Although modest yields of D-glucaric acid are obtained, due to competing side reactions generating numerous oxidation products, the method remains attractive for commercialization because of its relative simplicity with nitric acid serving as both solvent and source of the oxidizing agent. One of the most known commercial plant uses a proprietary technology developed by Rivertop that consists in a one-pot oxidation process without NO_x release (modification of the conventional process) [62].

Despite its commercial potential, large scale production of D-glucaric acid by nitric acid oxidation of D-glucose has been hindered, primarily due to competing side reactions which result in low selectivity toward the GA, moreover the low D-glucose conversion (<50% yield) and the rapid and highly exothermic character of the oxidation. The use of Au heterogeneous catalysts is less common due to the hard conditions required for the consecutive oxidation of GO to GA (Fig. 1.11).

Alternative oxidization methods that have been reported include catalytic oxidation with oxygen using a platinum catalyst with a 50-60% yield and selectivity of 85-90% at neutral pH and an operating temperature between 80° and 120°C, in the case of Pt/SiO_2 catalyst [63] and chlorine and bromine based oxidations employing TEMPO (2,2,6,6-tetramethyl-piperidine-1-oxyl) (Fig. 1.18) as a catalyst [64] [65]. The metal catalyzed reaction shows slightly improved yields of D-glucaric acid (54% yield), while the

TEMPO-based oxidations report higher glucaric acid yields (70–90% yield) but require relatively expensive oxidizing agents.

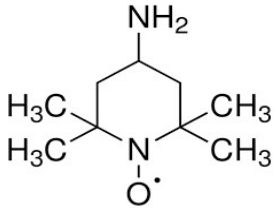

Figure 18: Structure of TEMPO

Biochemical production of D-glucaric acid has also been demonstrated using a process that first converts myo-inositol to D-glucuronic acid followed by an enzymatic or metal-catalyzed oxidation to D-glucaric acid [66]. A second reported biological synthetic route to D-glucaric acid originates from D-glucose in recombinant Escherichia coli [67].
Due to the increasing interest on the implementation of sustainability onto the industrial processes, recently electrochemical methods for the oxidation of glucose to GO and GA are under development.

1.7 Electrocatalysis

Electrocatalysis results in the modification of the rate of an electrochemical reaction occurring on an electrode surface. The electrocatalyst influences the reaction rate, the process efficiency and selectivity.
Interfacial charge transfer during an electrochemical reaction involves one of two possible mechanisms. The first kind, referred to as outer-sphere reactions, involves exchange of electrons between the electrode and the reacting species, with only very weak or no direct interaction between them. In this case, the kinetics and thermodynamics of charge transfer are insensitive on the electronic structure of the electrode [68] [69].
In the second type of interfacial charge transfer, inner-sphere reactions, there is significant interaction between the electrode and the reacting species, which may also involve the breakage and formation of bonds. The rate of the electrochemical reaction is extremely sensitive on the electrode surface properties [70] [71]. Only inner-sphere electron transfer reactions are thus relevant from the viewpoint of electrocatalysis.

In bulk electrodes, the surface is directly involved in the catalytic reaction. While in modified electrodes an active phase is deposited on the electrode, and two different interfaces can be formed: the electrode–catalyst interface and the catalyst–electrolyte interface.

If mass transport is assumed to be non-limiting and properties of the double-layer region are insignificant, for a given electrochemical reaction, then the rate of the reaction will be controlled by the rate of electron transfer across the electrode–catalyst interface. The use of a conductive matrix as support for catalyst particles, or encapsulation of the catalyst particles in a conductive matrix, typically carbon-based materials, usually results in substantial enhancement of electrocatalysis derived from improved charge transfer [72] [73].

The kinetics of faradaic processes are strictly dependent on the applied potential when they are performed on the electrode surface. There are two contributions on it: the thermodynamic one, described by the Nernst law and the kinetics one, from which is possible to have an idea of the energy dissipation, due to the existence of an overpotential (η). Designing the properties of an electrochemical interface, such as the geometric and surface electronic properties of the electrode, and tuning the structure of the double-layer is possible to maximize the rate of the electrochemical reaction of interest and minimize the reaction overpotential.

The general form of the electrochemical rate constant (k) of an electrode catalyzed reaction is given by the Arrhenius law:

$$k = A_0 e^{\frac{-\Delta G^{\ddagger}}{RT}} \tag{1.1}$$

Where A_0 is the pre-exponential factor, $\Delta G^{\ddagger}$ is the free energy of the reaction, R is the universal gas constant and T is the absolute temperature. The rate equation states that there are three options to increase the k, namely, increasing the pre-exponential term, increasing the reaction temperature, or decreasing the Gibbs free energy of the reaction. For a multi-step reaction, the ΔG term is connected with the activation energies of the various elementary steps involved. The goal of electrocatalysis therefore is to decrease the barrier to the reaction by minimizing the activation energy of the rate-limiting step.

Determination of the rate-limiting step is relatively easy for simple reactions such as the evolution of the oxygen (OER) and the evolution of the hydrogen (HER), while rather complicated for multi-step, multi-electron transfer reactions. The rate-limiting step may

be only marginally slower than some other elementary step; thus, a secondary low step can emerges upon overcoming the energy barrier of the primary limiting reaction.

1.7.1 Hydrolysis of water and Oxygen evolution

In general, the overall water splitting process can be represented as follows (equation 1.2) with molecular hydrogen and oxygen generated individually at the cathode and anode, respectively.

$$2H_2O + \text{Energy} \rightarrow 2H_2 + O_2 \quad (1.2)$$

In principle, the energy required to drive the water splitting reaction can be obtained from different sources making it a highly versatile energy conversion technology. For example, it is possible to couple electrochemical water splitting devices with renewable energy harvesting technologies, such as photovoltaic pannels and wind turbines.
In the water splitting system it should be considered the fundamental operating requirement that means that in order to generate hydrogen at a specific rate, a voltage at least equal in magnitude to 1.23 V must be supplied to the system. For water electrolysis, this operational voltage depends on the kinetics of the water splitting reactions and the design of the electrolyser unit such that (equation 1.3):

$$V_{op} = V_{eq} + \eta_A + |\eta_C| + \eta_\Omega \quad (1.3)$$

Where V_{op} is the operational voltage, V_{eq} η_A and η_C are the overpotentials required to overcome the kinetic barriers for the oxygen evolution reaction (OER) at the anode and the hydrogen evolution reaction (HER) at the cathode, respectively, and η_Ω is the additional overpotential required to compensate for resistance losses within the device [74]. In an ideal system η_A and η_C would be close to zero and V_{op} would depend only on η_Ω, which could be minimised through efficient design of the electrolyser unit. In alkaline solution, the OER (equation 1.4) and HER (equation 1.5) can be described by the following two electrochemical reactions:

$4OH^- \rightarrow O_2 + 2H_2O + 4e^-$ (V_{Anode} = 1,23 V vs RHE) (1.4)

$4H_2O + 4e^- \rightarrow 2H_2 + 4OH^-$ ($V_{Cathode}$ = 0 vs RHE) (1.5)

Where V_{Anode} and $V_{Cathode}$ are the equilibrium potentials for the OER and HER, respectively.

Due to the fact that the OER will take significantly part the glucose oxidation reaction, the reaction pathway, in alkaline solution, is written here below (equations 1.6-1.10):

$* + OH^- \rightarrow *OH + e^-$ (1.6)

$*OH + OH^- \rightarrow H_2O + *O + e^-$ (1.7)

$*O + OH^- \rightarrow *OHH + e^-$ (1.8)

$*OHH + OH^- \rightarrow *O_2 + e^-$ (1.9)

$*O_2 \rightarrow * + O_2$ (1.10)

Where * is the metal site.

The metal oxides, such as RuO_2 and IrO_2 and other noble metal (Pd, Pt, Au) oxides, thanks to their stability at the OER operating condition, are considered the best materials for catalysed the reaction [75].

Over the years various possible reaction pathways have been proposed. In the early mechanisms the OER was usually interpreted in terms of an initial discharge of hydroxide ions at a catalytically active surface site of the Metal (M), leading to the formation of adsorbed hydroxide intermediates (equation 1.11):

M + OH- → MOH + e- (1.11)

Subsequent steps in the reaction were thought to involve the formation of a range of surface adsorbed intermediates such as MO, MOOH or physisorbed peroxide species, which could then react with each other, through various disproportion or bimolecular decomposition reactions, or undergo nucleophilic attack from the electrolyte to liberate oxygen gas, as it is shown in Fig. 1.19, in the case of the OER catalysed by Pt [76].

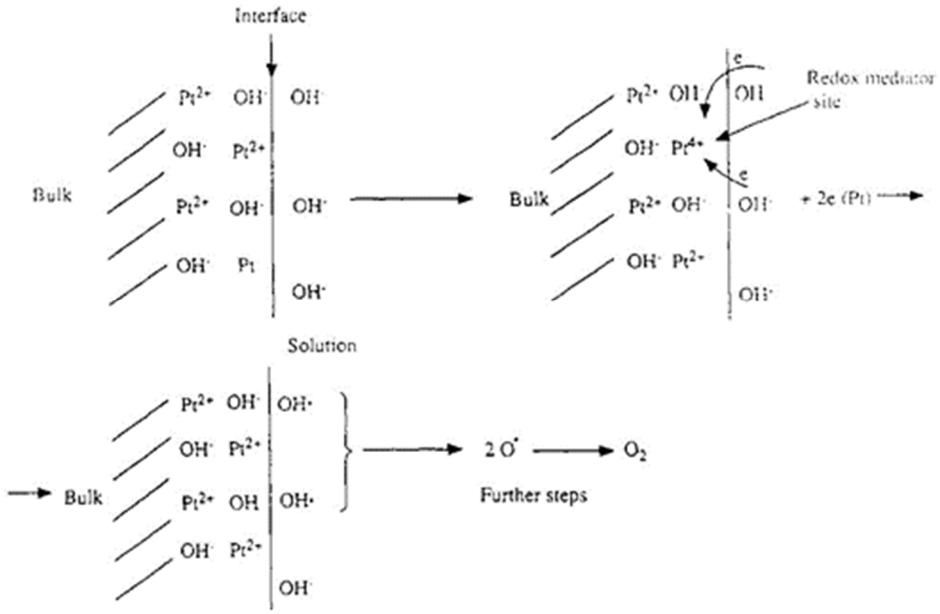

Figure 1.19: schematic representation of the OER acting on Pt catalyst *[77]*

The OER is the main concurrent reaction for the electrocatalytic oxidation of the glucose (GOR), this results in a decrease of the efficiency of the selective electrons transfer for the formation of the desired product. Furthermore, the formation of bubbles at the anode lead to less interaction between the electrolyte and the catalyst, resulting in a lower efficiency.

1.7.2 Electrocatalytic oxidation

Thanks to the promising progress on the use of electrochemical technologies in the abatement of bio-refractory substances, many studies on the electrochemical oxidation of organic matter for the remediation of wastewater have been carried out. These processes have shown high efficiency, mild operating conditions, ease of automation, versatility, and low cost, especially when they are powered by renewable energy from wind and solar sources [78].

Early mechanistic studies suggested that oxidation of organic pollutants involves O-transfer reactions at high anodic potential, via the production of adsorbed •OH generated from water discharge reactions, equations 1.12 and 1.13, where S[ ] represents the surface sites where the •OH species can be adsorbed (25):

$$S[\,] + H_2O \rightarrow S[\bullet OH] + H^+ + e^- \qquad (1.12)$$

$$S[\bullet OH] + R \rightarrow S[\,] + RO + H^+ + e^- \quad (1.13)$$

The undesirable OER occurs concomitantly as follows (equation 1.14):

$$S[\bullet OH] + H_2O \rightarrow S[\,] + O_2 + 3H^+ + 3e^- \quad (1.14)$$

A model proposed in 1994, shown a simplified mechanism for the selective oxidation or combustion of organics, with simultaneous O_2 evolution; the materials used for the anode were Pt, Ti/IrO_2 and Ti/SnO_2 [79].

In accordance with the literature, selective oxidation of organics occurs with electrodes forming the so-called higher oxide, MO_{x+1}, whereas combustion occurs with electrodes that allow the accumulation of •OH radicals on the surface. Pt and IrO_2 anodes favour selective oxidation because the •OH concentration is almost zero, while SnO_2 promotes complete combustion because of the significant accumulation of •OH radicals at its surface [79] [80].

From these studies it can be deduced that the electrochemical activity (which is related to the overpotential for O_2 evolution) and chemical reactivity (which is related to the rate of organics oxidation) of physisorbed M(•OH) are highly dependent on the strength of the M–•OH interaction [81] [82]. Thus, while anodes with low O_2 evolution overpotential lead to the partial oxidation of organics, anodes with high O_2 evolution overpotential favour the complete oxidation of organics to CO_2, thus becoming ideal electrodes for wastewater treatment, but not for the selective oxidation of molecules.

1.7.3 Electrocatalytic oxidation of glucose for sensors

Biosensors for glucose monitoring uses the protein glucose oxidase, that generates an oxidation current upon reaction with glucose. Grafting the enzyme on an electrode allows the determination of oxidation current and, hence, glucose levels.

There are three different sensors commonly used:

- Enzymatic
- Microbial
- Abiotic or not enzymatic

For the purpose of this work only the third category will be explained.

The abiotic electro-oxidation of the glucose was performed using different compounds such as: metals (Pt, Au, Pd, Cu, Ni, Ag, Fe, Co), metal oxides and hydroxides (RuO_2, $Ni(OH)_2$, MnO_2), alloys (PtPb, PtRu) and material based on carbon (reduced graphene oxide, rGO, carbon nanotubes) [83].

There are two different types of approaches that describe the electrocatalytic process between electrode and glucose. The first suggests that the reaction takes place in a concerted manner: the hemiacetalic hydrogen is tear off simultaneously with the adsorption of the glucose. In fact, the determining step in many glucose electro-oxidation experiments is believed to be the removal of the hydrogen atom [84] (Fig. 1.20).

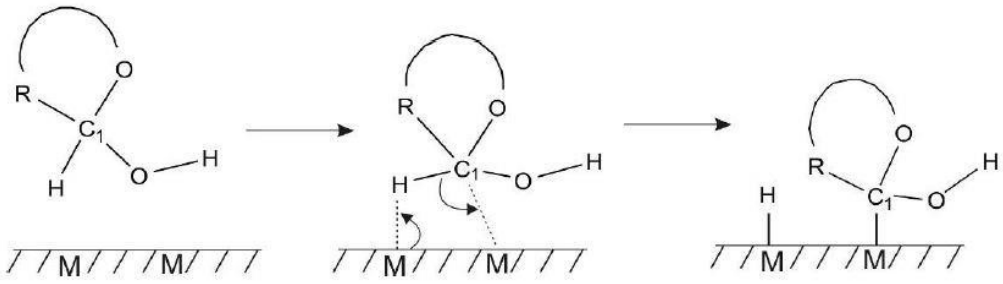

Figure 1.20: concerted adsorption mechanism, with simultaneously hydrogen remove, proposed by Pletsher *[85]*.

This approach does not take in account the oxidant role of hydroxylic radicals. For this reason a second model was proposed. This model states that the electrooxidation of glucose and other organic molecules corresponds with the OH_{ads} adsorption onset [86]. This model, called IHOAM (Incipient Hydrous Oxide Adatom Mediator) presents a first step of premonolayer oxidation of the active phase of the metal atoms, with the formation of an incipient layer of hydrate oxides with reactive OH_{ads}, that mediate the oxidation and increase the reaction kinetics [87].

The premonolayer therefore acts as a mediator of the oxidation of the adsorbed species to lower potentials than normal ones [86]. (Fig. 1.21).

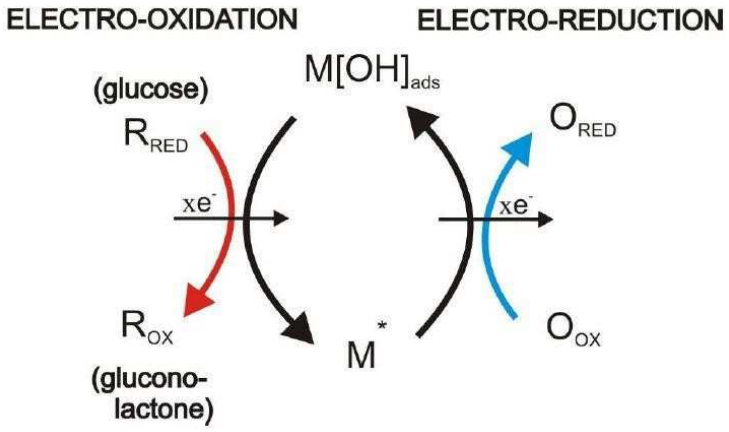

Figure 1.21: Schematic illustration of the IHOAM model in which M* is the reducing metallic site and MOH_{ads} is the adsorbed hydroxyl radical *[85]*.

It seems that the IHOAM model is the basis of the mechanism for catalysts such as Pt, Ru, Au and Pd. The hydroxyl group also plays a role in the electrocatalysis of glucose over Ni and Cu electrodes; however, in this case the premonolayer is not formed to induce catalysis, but to induce a change in the oxidation state of the metal hydroxide.

Ni electrodes are not reported in the literature to be active in the reaction with neutral or acid pH, but it is with a basic media that report the maximum current density for the GOR [85], due to an easier formation of complexes MOH and MO, the main responsible for the electrochemical oxidation of glucose [88]. Moreover, it prevents the precipitation of organic acids that would cause catalyst poisoning and a reduction in process efficiency; it favours the presence of the β form of cyclic glucose (glucopiranose), considered more easily oxidizable than α; and the stability of metal-based electrodes or metal oxides is increased [40].

For the purpose of this work, only the mechanism that involves the Nickel species will be explained.

Nickel electrodes have been studied extensively as catalysts for the oxidation of organic molecules, such as glucose, in a basic media. Studies have shown that the catalytically active species is the oxyhydroxide of Ni (III), the oxidized partner of the redox pair $Ni(OH)_2$/NiOOH [89] [90]. This is produced by a change in the oxidation state of Ni on the electrode surface, as shown by the equation 1.15:

$$Ni(OH)_2 \rightarrow NiOOH + H^+ + e^- \qquad (1.15)$$

By immersing an electrode of Ni, or $Ni(OH)_2$ electrodeposited in an alkaline electrolyte, two crystallographic species are formed: the hydrated form, the α-$Ni(OH)_2$ and the anhydrous one, the β-$Ni(OH)_2$ [91] [92]. Between the two crystalline species, the most stable is the β, which is also the catalytically active one [93].

In deposited $Ni(OH)_2$ the two species α and β are not present in stoichiometric quantities. Cycles of variation of the potential in the basic environment lead to aging of the electrode, characterized by the shift of the potentials towards more anodic values and to an enrichment of the $Ni(OH)_2$ layer [94].

The oxidation of all organic molecules (glucose in our case) at the Ni electrode takes place immediately after the formation of the Ni(III) via the oxidation of $Ni(OH)_2$ to the catalytically active NiOOH (figure 1.22a), after that glucose undergoes hydrogen abstraction at the surface to form a radical intermediate and reforming the $Ni(OH)_2$ species (figure 1.22b), then hydroxyl anions in the solution rapidly complete the oxidation of the organic radical intermediate to form gluconolactone (figure 1.22c) [91].

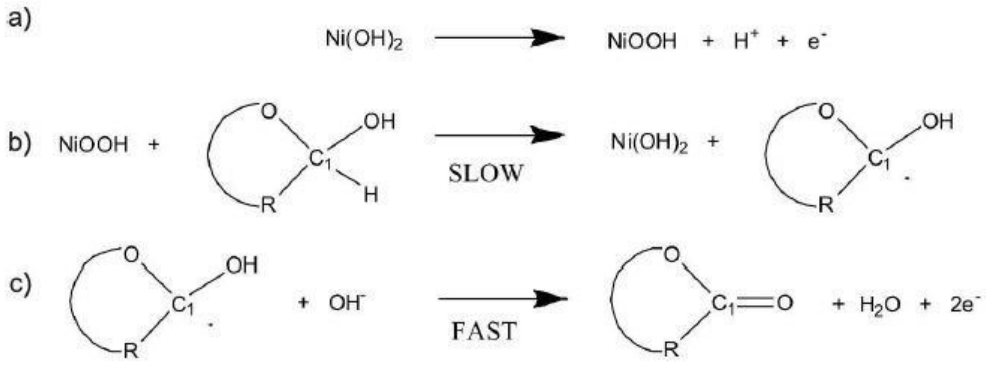

Figure 1.22: Suggested mechanism for glucose oxidation using a $Ni(OH)_2$ electrode in alkaline solution *[85]*.

The product of this reaction is identified as gluconolactone, which is subsequently hydrolyzed to gluconic acid. The oxidation appears to occur in the bulk of the electrolyte and not just limited to the interface between electrolyte and the electrode [95].

1.8 Selective oxidation of glucose to gluconic and glucaric acid

With the increasing research on the development of sensors for the diagnosis of diabetes, which take advantage of the electro-oxidation reaction of glucose to γ-gluconolactone

(the ester of gluconic acid), some studies have also reported the interest in selectively producing value-added molecules such as gluconic and glucaric acid.

The electrochemical method shows some advantages compared to the methods currently used for the conversion of glucose to gluconic and glucaric acid. Mild conditions can be used with low temperature and pressure without the employment of O_2 or HNO_3, avoiding also HNO_3 disposal or NOx abatement. The use of H_2O as source of oxygen therefore makes these processes more sustainable. The reaction can be controlled by adjusting the operating voltage or current density.

Nevertheless, the application of the electrochemical method in organic synthesis, and in particular for glucose oxidation, still presents some drawbacks. The efficiency and selectivity of the electrochemical reactions are limited by weak conductivity of the cell, poor mass transfer on the surface of the electrode and untimely separation of reactant and product.

The selectivity is the critical issue also for the electrochemical oxidation reaction of the glucose to gluconic and glucaric acid. Many different side reactions (Fig. 1.23) give rise to the formation of undesirable products that may also cause the poisoning of the catalyst.

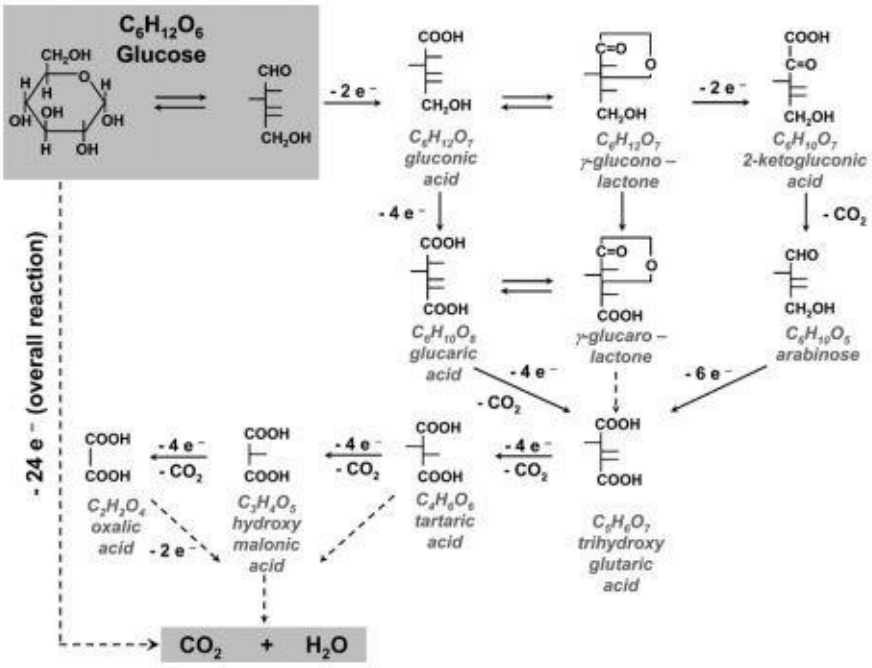

Figure 1.23: different routes in the glucose oxidation *[96]*

In the glucose oxidation reaction (GOR) for every molecule 24 electrons have to be released ($\Delta G° = -2780$ kJ mol^{-1}) in order to achieve the complete oxidation to CO_2:

$$C_6H_{12}O_6 + 6O_2 \rightarrow 6CO_2 + 6H_2O \quad (1.16)$$

The selective oxidation to gluconic acid only requests 2 electrons ($\Delta G° = -2.51 \times 105$ J mol^{-1}):

$$C_6H_{12}O_6 + 0.5O_2 \rightarrow C_6H_{12}O_7 \quad (1.17)$$

$$C_6H_{12}O_6 + 2OH^- \rightarrow C_6H_{12}O_7 + H_2O + 2e^- \quad \text{(anodic half reaction)} \quad (1.18)$$

The reduction potential can vary due to the electrocatalyst, the applied temperature and pH conditions. For Ni, for example, electrodes the potential at which the glucose oxidation occurs is between 0.4 and 0.6 V vs Ag/AgCl [97].
In the following equations is presented the reaction scheme for the oxidation of gluconic acid to glucaric one.

$$C_6H_{12}O_7 + 0.5O_2 \rightarrow C_6H_{10}O_8 + H_2 \quad (1.19)$$

$$C_6H_{12}O_7 + 4OH^- \rightarrow C_6H_{10}O_8 + 3H_2O + 4e^- \quad \text{(anodic half reaction)} \quad (1.20)$$

Recently, a MnO_2/Ti tube-shaped and porous electrocatalytic flow reactor has been developed to perform, selectively, the GOR at neutral value of pH. The results show that with a loading of 0.85 wt% of the MnO_2 and a current density of 3mA/cm^2 the glucose conversion is 55% and total selectivity to GO and GA over 90% with a current efficiency of the 48% [98].
Another significant study about this process employs an homogeneous catalyst, TEMPO, in a NaBr water solution with graphite anode and a stainless still cathode obtaining a yield of 85% in the GA; however the high costs and the difficulty on the recycling of the catalyst make this process unsuitable for the industrial application [65].

1.9 Electrocatalyst with high surface area

There are two approaches for increasing the activity of an electrocatalytic system:

- Increase the number of active sites on the electrode, raising the amount of active phase or modifying the catalysts structure.
- Increase the activity of the individual active site.

Open cell metallic foams can be employed directly as catalyst or as 3D support on which depositing an active phase. Compared with other 2D metallic supports, foams have a highly macroporous structure, providing a larger surface area, more active sites and enhanced electrolyte penetration and gas diffusion. Its conductive and continuous 3D framework enables excellent mechanical strength and fast electron-transfer pathways, resulting in increased intensity current values.

The use of commercial 3D macroporous materials such as Ni foam, FeNi foam, Cu foam, carbon foam, graphene foam, etc., have been brought to the forefront in electrocatalysis in recent years for their flexible uses in process such as HER, OER, overall water splitting, oxygen reduction reaction (ORR) and methanol oxidation reaction (MOR) [99].

1.9.1 Deposition methods

The methods that are generally applied for the deposition of active phase on electrodes are based on chemical, spontaneous or electrochemical deposition.

The efficiency of the structured catalysts will depend on both the properties of the deposited material (amount, composition, size and dispersion of the active species) and the adhesion of the deposits to the support.

There are many techniques for the deposition of metal particles or metal oxides on a support, three of them are listed below:

- Chemical vapor deposition: it is a technique that allows the formation of ultrathin metal films through the reaction in gas phase between the active phase precursors, generally hydride or chloride of the metal, directly onto the surface [100].
- Galvanic displacement: it involve a single step reaction where metallic ions are spontaneously reduced and deposited on the substrate that is consequently oxidised [101].
- Electrodeposition: it is an electrochemical process that involves the current for the reduction of the metal ions presented on the solution or

other species that generate a basic media, allowing the deposition of metallic particles or hydroxides/oxides on the electrode.

In this work, we investigated the electrodeposition method due to its easily applicability in aqueous phase and low costs.

This method is widely employed for the deposition, on conductive supports, of metal particles, hydroxides or oxides, in a single step and at room temperature. Metal electrodeposition starts on extraneous electrodes with the formation of individual growth centres until a continuous or disperse layer is produced [102].

The morphology and the thickness of the deposited material layer can vary due to several factors: time of deposition, [56] concentration of the active species, applied potential, support material, solution temperature, the stirring of the solution and the degree of purity of the electrolyte.

For the deposition of metal particles it is necessary that the applied potential and the solution are chosen to reduce the metal precursors efficiently and selectively (eq. 1.21):

$$M_{z+(solution)} + ze^- \rightarrow M_{(surface)} \quad (1.21)$$

With e^- depending on the type of metal

The electro-base generation method is used for the deposition of oxides and hydroxides. During the electrodeposition the reduction of species such as NO_3^- and H_2O, (Fig. 1.24), produce a local increase of the pH due the presence of the OH^- ions in the interphase between the electrode and the electrolyte, resulting in the chemical precipitation of cations present in the solution directly on the electrode surface as oxides and hydroxides. Some examples are oxides and hydroxides of metals such as Ni, Al, Fe, Co, Cr, Mg, Rh [103] [104].

Reaction		Potential E° (V)
1)	$NO_3^- + 2H^+ + 2e^- \rightarrow NO_2^- + 2H_2O$	0.934
2)	$NO_3^- + 2H_2O + 2e^- \rightarrow NO_2^- + 2OH^-$	0.010
3)	$NO_3^- + 10H^+ + 8e^- \rightarrow NH_4^+ + 3H_2O$	0.360
4)	$NO_3^- + 7H_2O + 8e^- \rightarrow NH_4^+ + 10OH^-$	-0.120
5)	$2H_3O^+ + 2e^- \rightarrow H_2 + 2H_2O$	0.000
6)	$2H_2O + 2e^- \rightarrow H_2 + 2OH^-$	-0.828
7)	$O_2 + 2H^+ + 2e^- \rightarrow H_2O_2$	0.695
8)	$H_2O_2 + 2H^+ + 2e^- \rightarrow 2H_2O$	1.776
9)	$O_2 + 4H^+ + 4e^- \rightarrow 2H_2O$	1.229
10)	$O_2 + H_2O + 2e^- \rightarrow HO_2^- + OH^-$	-0.076
11)	$HO_2^- + H_2O + 2e^- \rightarrow 3OH^-$	0.878
12)	$O_2 + H_2O + 4e^- \rightarrow 4OH^-$	0.401

Figure 1.24: electrochemical reduction reactions of nitrate, H_2O and O_2 involved in electrodeposition processes of metal oxides and hydroxides. *[104]*

2. Experimental part

2.1 Material and reagents

The list of materials and reagents, for the synthesis of the electrocatalysts and for their use in catalytic tests, is shown in table 2.1.

Table 2.1: list of materials and reagents used

Compound	State of the matter	Molar mass (g/mol)	Purity (%)	Supplier
NaOH	Pellets	40,00	98	Sigma-Aldrich
Glucosio	White solid	180,156	99	Alpha-Aesar
$Ni(NO_3)_2*6H_2O$	Green solid	290,81	99,8	Alpha-Aesar
Ni metal foam	Macroporous solid	-	-	Alantum
HCl	Aqueous solution	36,46	36%	Sigma-Aldrich
2-propanol	Liquid	60,09	100	Sigma-Aldrich

All the aqueous solutions were prepared using ultrapure water obtained with the Milli-Q plus system (Millipore Co, resistivity 18.2 MΩ cm).

2.2 Electrocatalysts preparation

The catalysts used for the electrochemical tests are based on 3D open cell nickel foams. These supports were tested as bulk materials and support on which a different active phase was deposited.

The support used for the foams was obtained from Ni macroporous sheets of 300 mm x 200 mm x 1.6 mm with a cell size of 450 µm, from which foam pieces of 10 mm x 10 mm size were obtained. Then these foams were fixed to a glass stick through a platinum contact that connects also the foam piece to the instrument.

For the foam used as bulk or as support before any operation they were pre-treated via a washing cycle composed by washing with UPP water and isopropanol for 1 min, with

HCl 1M for 5 min, then again with water. At this point the support was ready for the deposition of the active phase and/or for the electrochemical tests.

The deposition of $Ni(OH)_2$ was performed in a double compartment three-electrode flow cell.connected to potentiostat/galvanostat Metrohm Autolab PGSTAT204 with NOVA software. The working electrode (WE) is the foam, while the reference electrode (RE) is made by saturated calomel electrode (SCE) and the counter electrode (CE) is a platinum gauze. The electrodeposition was performed at -1.2 V vs SCE for 50s. The electrolyte was an aqueous solution of $Ni(NO_3)_2$ 0.10M.

Moreover, cleaned foams were calcined in a muffle furnace, Lenton, at 500 or 650 °C for 1 h (10°C/min heating ramp).

2.3 Characterization techniques

2.3.1 SEM

To study the morphology of our samples, SEM (Scanning Electron Microscope) analyses were performed, while an EDX (Energy Dispersive X-Ray Spectroscopy) analysis was performed to determine the composition of the surface.

The SEM electron microscope is a device that allows to examine the surface of a sample at high magnifications and, since it uses an electron beam as a means to generate the image, it allows to reach a higher depth and resolution compared to normal optical microscopes.

At the same time, EDX can be exploited to obtain elementary semi-quantitative results on specific areas of the analyzed surface.

In a SEM the electron beam is generated by an electron gun, generally a tungsten hairpin filament which is heated to high temperatures to produce thermal emission of electrons from its tip; later on, the beam is focused through two lenses into a fine probe which is scanned across a selected area of the specimen surface in a raster by scan coils. The electrons penetrate the specimen in a teardrop-shaped volume whose overall dimensions are determined by the energy of the electron beam, the atomic masses of elements in the specimen and the angle at which the electron beam hits the specimen.

The interaction of the electron beam with the specimen produces secondary, backscattered and Auger electrons, x-rays and perhaps light, collected by various detectors in the specimen chamber.

Various signals from the specimen can be collected and used to form images:

1. Secondary Electrons are those that escape from the specimen with energies below 50 eV mainly knocked out of their orbits around an atom by an incident electron. These provide the highest spatial resolution images; the signal comes from an area about the size of the electron probe. The SEM images are greyscale with respect to color because the detected electrons have a wavelength that does not match within the visible spectrum. The contrast between the different shades of gray color gives an idea of the depth of the image.
2. Backscattered electrons are those incident electrons that approach the nucleus of an atom sufficiently closely to be scattered through a large angle and re-emerge from the surface. They are not as numerous as secondary electrons but have much higher energies. Images have slightly less resolution than that of secondary electron images because they come from slightly deeper in the specimen, resulting in an area larger than the probe size. They provide compositional information: elements of higher atomic mass give brighter contrast.
3. Auger electrons are emitted from atomic layers very close to the surface and give valuable information about the surface chemistry. Due to their low numbers they required dedicated instruments and advanced detectors.
4. Characteristic x-rays are generated by atoms when the incident high-energy particle knocks out an inner-shell electron and an outer-shell electron moves into the empty orbit. Measurement of the energies of these x-rays gives information about the chemical composition of the specimen. EDX is the more common analytical technique coupled to SEMs as it provides rapid semiquantitative analysis of the specimen [105].

The scanning electron microscope used for our analysis was an EVO 50 EP (LEO ZEISS), with an energy dispersed microprobe (EDX) Oxford Instruments INCA ENERGY 350 equipped with an INCASmartMap system.

The applied potential difference for the electron acceleration was 20 kV and the acquisition time of the spectra for the EDX analysis of 60 seconds.

2.3.2 Raman Spectroscopy

When a monochromatic radiation hits a surface, part of it is absorbed, part is reflected and finally a small part is diffused. The latter partially is diffused with an elastic collision mechanism, without energy variation (Rayleigh scattering), maintaining the same frequency of the incoming beam. The remaining fraction instead, due to inelastic collision, is diffused with a different energy and therefore also a different frequency (Raman scattering). This phenomenon is due to the variation of polarizability (ability to create a short-lived dipole) of the atoms present in the sample, induced by the vibrational transitions caused by an incident laser radiation (in the visible spectra).

If a vibration can cause periodic polarizability variations (for example by expanding or contracting the electronic cloud), then the diffused radiation can contain the frequency of this vibration superimposed (+ or -) on that of the incident wave. In both elastic and inelastic interactions, one can imagine that the molecules affected pass from a virtual energetic state $h\nu_0$ from which they decay emitting photons.

The inelastic interaction can evolve into two distinct pathways:

- The molecule decays to an excited vibrational energy state emitting a photon of energy lower than that of the incident wave (Stokes shift, towards red);
- The molecule already presents in an excited vibrational state, decays from the virtual state to the ground state, emitting a photon of energy greater than the incident one (anti-Stocks shift, towards blue).

At room temperature the most populated vibrational level is the fundamental one, then anti-Stokes shifts are less frequent than Stokes ones. What is measured is therefore the difference between the frequency of the incident radiation and the scattered radiation [106].

The instrument used is a Renishaw RM1000 micro-spectrometer. The experiment is carried out by focusing the objective at 50x magnification in the area of interest, proceeding by making the laser engraved and making the measurement. A green laser (Ar^+ 514.5 nm) is used with 10% power. Spectra were recorded between 4000 and 100 cm^{-1} for the analysis of the foams with Ni electrodeposited and between 2000 and 1000 cm^{-1} for the bare foams, with 4 accumulations and acquisition time of 10 seconds.

2.3.3 X-ray Diffraction

The XRD (X-ray diffraction) technique is used to study the crystal structure of substances. It can be used for a mono-crystalline sample or, if it is not possible to prepare a single crystal, its variant can be used, which includes the analysis of powder, called PXRD. A simple and effective way to approach diffraction is through the law of Bragg.
It describes the interaction between an incident wave with atoms arranged on a crystalline plane with Miller indices h = (hkl) and distance between the planes d_h. In order to a constructive interference to occur between the diffracting radiations of two atoms arranged one above the other in two crystalline planes, the difference of length of the optical path identified by a refraction angle θ must be a multiple of the wavelength λ according to the law [107]:

$$2d_h \sin\theta = n\lambda \qquad (2.1)$$

with n = 1,2 ...

Refer to figure 2.1 for a better understanding.

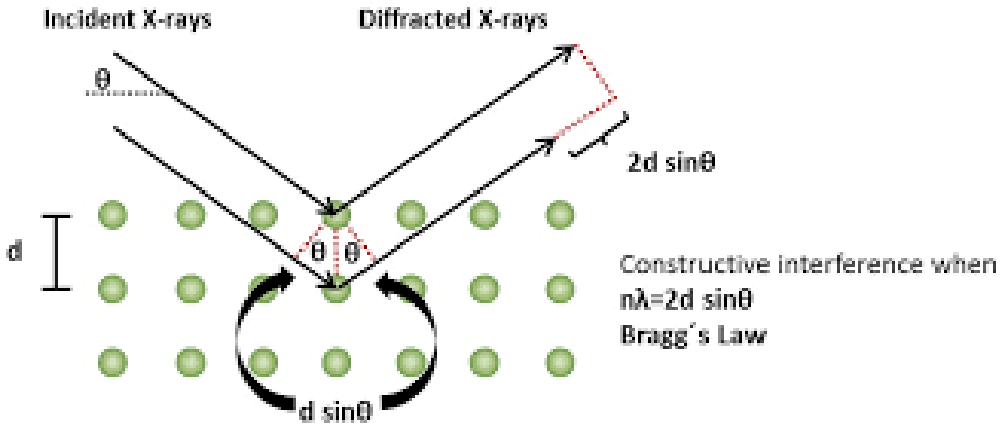

Figure 2.1: Explanation of the bragg law

The analyses were performed with a PANanalytical Xpert diffractometer with Xcelerator detector, which uses a copper anode (Kα, λ = 0.15418 nm) as X-ray source. The measurements for the foams were carried out on an interval of 2θ with a step size of 0.067° and time per step of 60.95s

2.4 Electrochemical test

The electrochemical tests were carried out in a three compartments cell, as in Fig. 2.2, in the central compartment the working electrode (WE), foams, and the reference electrode (RE) were inserted. The RE is inserted in a Luggin type capillary arranged with a distance of almost 2mm from the working electrode. In the side compartments platinum gauzes that constitute the counter electrode (CE) are inserted.

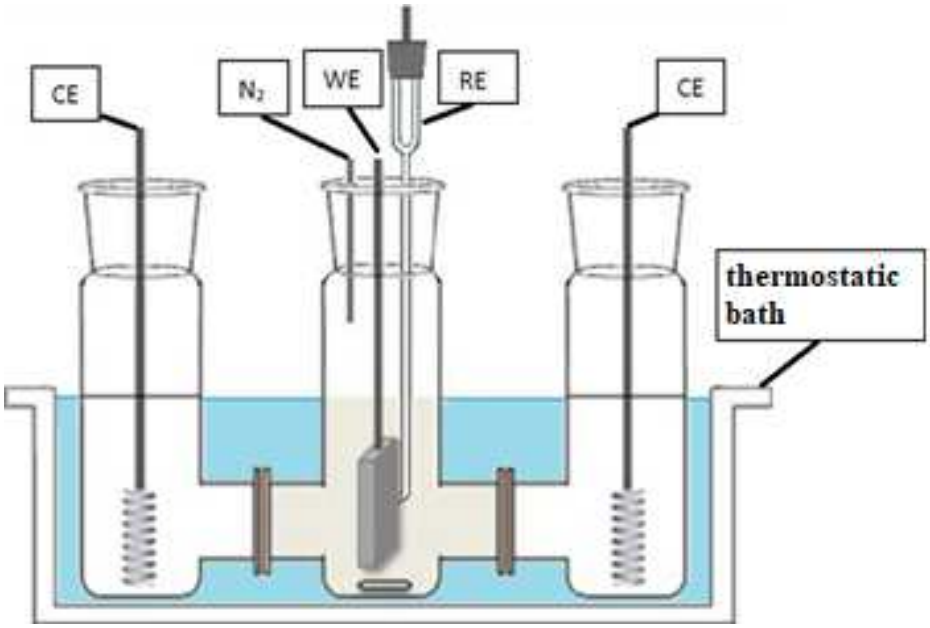

Figure 2.2: set-up of the three-compartment electrochemical cell

The working electrode is the electrocatalyst on which the reaction of interest takes place. The reference electrode has a stable and well-known electrode potential, so it is used for measuring the potentials in the electrochemical cell. In the calomel electrode with saturated KCl the redox potential is +0.2444 V vs. SHE at 25 °C.

The counter-electrode is used to guarantee the current flow inside the electrochemical cell and usually does not participate in the reaction. The cell was connected to a potentiostat/galvanostat, Metrohm Autolab PGSTAT204, which accurately controls the potential between the CE and the WE in a way that the potential difference between the WE and the RE is well defined and corresponds to the chosen value; the cell was kept in a thermostatic bath fixed at 25°C, in order to avoid the influences of the temperature on the tests.

Electrochemical tests were performed using 10 to 100 mM D-glucose aqueous solutions in 0.1 M NaOH (pH = 13),. In order to remove the dissolved oxygen, gas N_2 was flushed in each solution before use. The electrolytic solution (25mL) was poured into the central compartment, while in the two side compartments a solution of NaOH 0.1M was introduced.

To study the catalytic activity of electrocatalysts in the glucose oxidation, cyclic voltammetry (CV) tests were performed. Cyclic voltammetry is a voltammetry technique where the potential between the working electrode and the reference electrode is varied linearly over time, within a defined range of potentials. The speed at which the potential is varied (scanning rate) is therefore constant throughout the potential range, in our reaction was settled at 5 mV / s.

What is recorded is a current of variable intensity based on the electrochemical processes involved, which can vary according to the applied potential, obtaining a voltammogram. With the variation of the potential the analyte can undergo oxidation or reduction, through an exchange of electrons with the working electrode, which results in a peak in the voltammogram: positive in the case of an oxidation and negative for reduction processes. If there are reversible processes, when the voltage returns to the value for which the analyte already oxidized/reduced in the first scan is respectively reduced/oxidized, a new peak is recorded in the voltammogram with a similar shape to the previous one, but with a polarity opposite and the pair of peaks, in the case of a single electronic transfer reaction, will be separated by a maximum potential difference ΔE of 57 mV. From this it is possible to derive the redox potential of a redox pair ± any overvoltages caused by the system and information regarding the speed of the reaction. Unlike the LSV (linear scanning voltammetry, another similar technique for electrochemical investigations) in the CV the variation of the potential does not end when this reaches a given maximum or minimum value, but when the trend is reversed. This inversion can occur several times during a single experiment, a technique generally used to evaluate the properties of an analyte in solution, as well as for the study of redox systems in solid state and surface chemistry [108].

The chronoamperometry (CA) is an analytical technique, in which a current is measured and recorded as a function of time. A potential is applied between the working electrode and the reference electrode that can be constant or follow a programmed scheme, and the current recorded in the chosen time interval embodies the faradic processes that take place.

In the present thesis work, each cyclic voltammetry was performed by carrying out 3 scans, from -0.4 V to 0.8 V and back to -0.4 V at 5 mV/s scan rate.
The chronoamperometries were performed at our foams using 3 different anodic potentials: 0.6 V, 0.7 V and 0.8 V vs SCE, with a constant agitation of 1000 rpm. All processes were conducted at ambient T and atmospheric P.
At the end of the scans the catalysts and the cell are washed with UPP water.

2.5 Analysis of reaction products

2.5.1 High-performance liquid chromatography (HPLC)

The obtained reaction mixture was analysed by high performance liquid chromatography (HPLC). It is a chromatographic technique mainly used for analytes that are not very volatile or thermally unstable, but that are soluble in a solvent (eluent) potentially usable for analysis. The solution, composed by the analyte and the eluent (or by a mixture of eluents), defined as a mobile phase, is pumped at high pressure through a column packed with chromatographic material, the stationary phase. As the flow passes through the column, the analytes interact between the two phases at different speeds, due to the different polarity and size. The separation of the analytes in a homogeneous system therefore depends on the affinity of the analytes towards one or the other phase: the compounds that show a poor interaction with the stationary phase or a good interaction with the mobile phase will come out more quickly from the column, so they will have a shorter retention time. In order to be able to reveal the analytes and perform a quali-quantitative analysis, a detector is used, that sends the information to a computer that transforms the information into a chromatogram.
The instrument used is an Agilent Technologies 1260 Infinity HPLC with Series autosampler, equipped with a DAD (Diode Array Detector) UV-Visible detector set at a wavelength of 202nm for the detection of organic acids and a RID (Refractive Index Detector) thermostat set at 40°C for the detection of monosaccharides. For the analytical separation of the products two Rezex ROA-H + (8%) 300x7.8 mm columns were used consecutively. These columns are composed of nonpolar resins consisting of 8%

crosslinked styrenedivinylbenzene (SDVB) and branched with long hydrophobic chains ending with sulphonic acid groups (-H +).

With this type of columns, it is possible to obtain separations based on multiple modes of interaction between the mobile phase and the stationary phase, including ion exchange, ion exclusion, dimensional sieves and partition.

In many cases, the synergy between the various partition methods listed allows the separation of several classes of elements with a single column.

The two columns work in reverse phase, in which the molecules of the injected sample are distributed in an aqueous polar solvent, which acts as a mobile phase. While the stationary phase is represented by nonpolar molecules functionalized with acid groups. The analyses were conducted in isocratic conditions using 0.0025 M sulfuric acid in ultra-pure water as eluent (0.5 ml/min flow). The injection system consisted of a six-way valve with a sampling volume of 20 µl. The columns were thermostated at 80°C.

The DAD is a fixed or variable wavelength UV detector, in which the UV absorption of the effluent is continuously measured at single or multiple wavelengths. While the RID is a detector that measures the refractive index of an analyte with respect to the solvent. It is considered a universal detector because it can detect any substance with a refractive index different from the solvent but lacks low sensitivity. Both detectors are non-destructive to the sample subjected to the measurements.

In the chromatograms acquired with the DAD detector, the overlap between the glucose peaks and those of the gluconic acid occurred, however the glucose signal can be corrected by subtracting from the obtained concentration at the RID that of the gluconic acid obtained with the DAD. This method has been validated by injecting solutions with different known amounts of glucose and gluconic acid and verifying the existence of a correlation between the areas in the chromatogram and the theoretical ones.

Through the integration of the peaks and the construction of a calibration curve with aqueous solutions of known concentration prepared by commercial standards, the concentrations of GO and GA formed and of unconverted D-glucose were recovered.

Subsequently conversion, selectivity and faradic efficiency (FE) were calculated according to the following equations:

$$glucose\ conversion\ (\%) = \frac{converted\ mole\ of\ glucose}{initial\ mole\ of\ glucose} * 100 \quad (2.2)$$

$$selectivity\ of\ x\ (\%) = \frac{mole\ of\ x\ after\ the\ reaction}{converted\ mole\ of\ glucose} * 100 \quad (2.3)$$

Where x indicates the different products obtained and identified

$$FE\ gluconic\ ac.(\%) = \frac{mole\ of\ formed\ gluconic\ ac.}{total\ transfered\ charge} * (2 * F) * 100 \quad (2.4)$$

$$FE\ glucaric\ ac.(\%) = \frac{mole\ of\ formed\ glucaric\ ac.}{total\ transfered\ charge} * (2 * F) * 100 \quad (2.5)$$

With F as the Faraday constant = 96485.33 C/mol.

3. Results and discussion

The following chapter discusses and elaborates the results in the electrocatalytic-oxidation of glucose with 3D open cell foams of Ni, used as such or as supports for the deposition of an active phase.

Firstly, the results from the characterization of the foams before performing any test are presented. Then electrochemical characterization is shown, carried out by cyclic voltammetry (CV) in:

1. NaOH 0.1M solution at 5 mV/s, to investigate the oxygen evolution reaction and the redox species on the catalyst surface.
2. D-glucose 10 mM or 50 mM solution at 5 mV/s, to investigate the catalytic activity of the electrodes on glucose (onset potential for glucose oxidation and current densities).

For both CVs 3 scans were carried out each from -0.4V to 0.8V and back to -0.4V vs SCE.

3.1 Characterization of the metal foams

In this first section, the results obtained from the characterization of the different Ni foams will be discussed in order to have a first comparison between them.

The SEM image of the Ni bare foam, Fig. 3.1, shows a macroporous structure (a) and the irregular surface (b) with the presence of grain boundaries. The EDS analysis confirms the presence of the metal Ni.

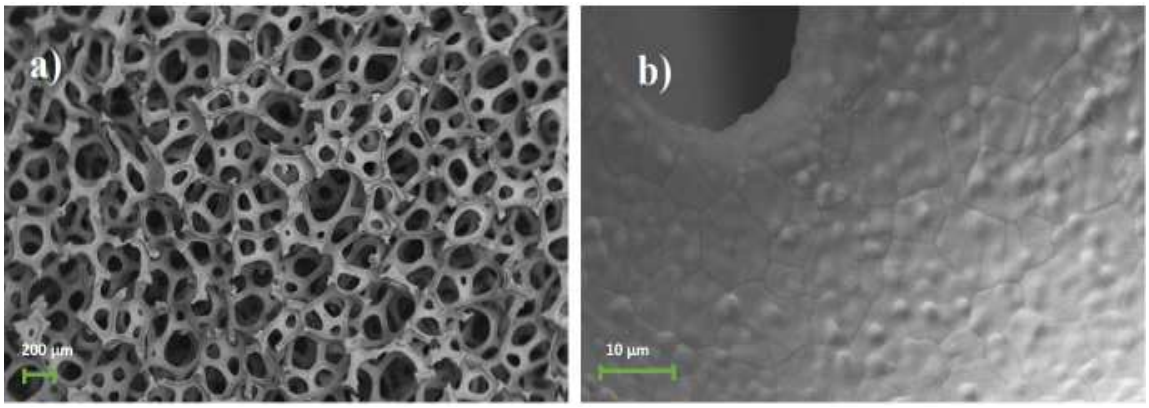

Figure 3.1: SEM images of a Ni bare foam at different magnification

After the calcination treatment, Fig. 3.2, at 500°C a slight modification of the surface can be observed due the formation of a surface oxide. EDS analyses suggest the presence of Ni oxides on the surface, in fact the amount of Oxygen is around the 34% in atomic percentage.

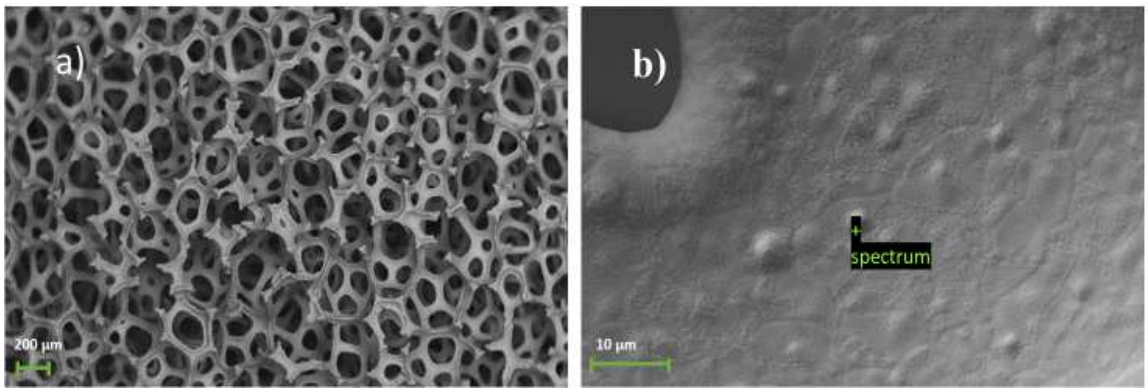

Figure 3.2: SEM images of Ni foam calcinated at 500°C at different magnification

The presence of NiO on the surface of the catalyst is confirmed by micro-Raman and XRD (Fig. 3.3-3.4). The spectra of the catalyst surface show two bands at 532 cm^{-1} related to one phonon LO mode and 1100 cm^{-1} related to two phonon 2LO mode of NiO, while the band at 1503 cm^{-1} is associated to a two-magnon (2M) excitation [109]. The XRD diffraction pattern (Fig. 3.4) shows the presence of low intensity reflections at around 37°, 43° and 63° that correspond to NiO.

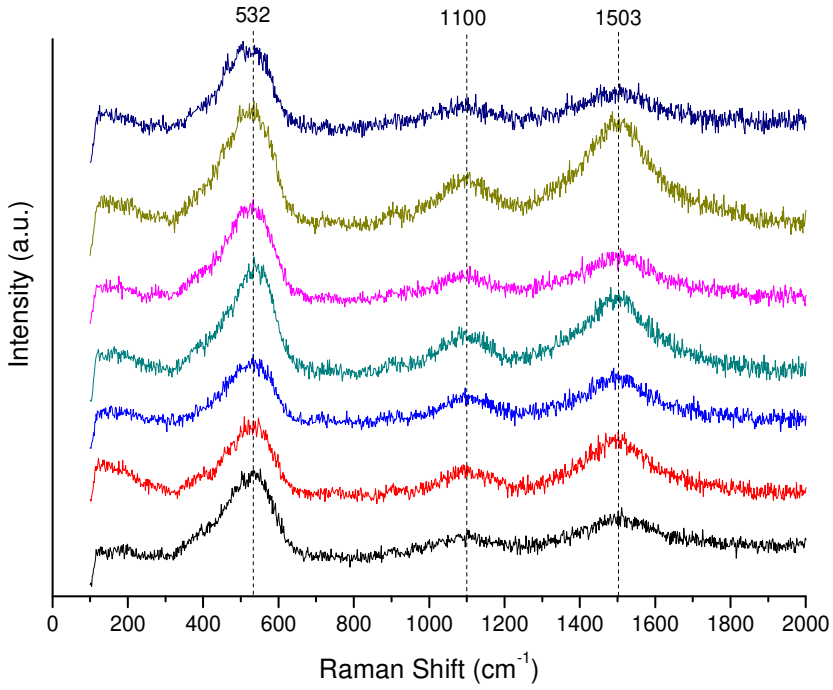

Figure 3.3: Raman spectra of a Ni foam calcinated at 500°C

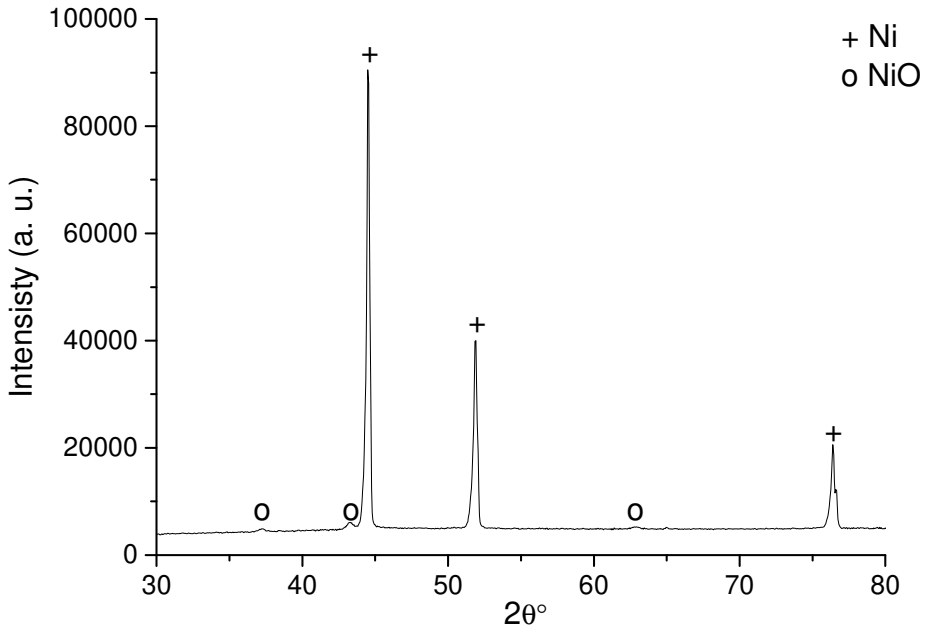

Figure 3.4: XRD pattern of a Ni foam calcinated at 500°C

Unlike at 500°C, the morphology of the foam surface changes after calcination at 650 °C. An irregular layer of nickel oxide develops (Fig. 3.5b), probably due a higher temperature of calcination. The largest amount of O measured by EDS (57%), suggests a higher degree of oxidation of the metal.

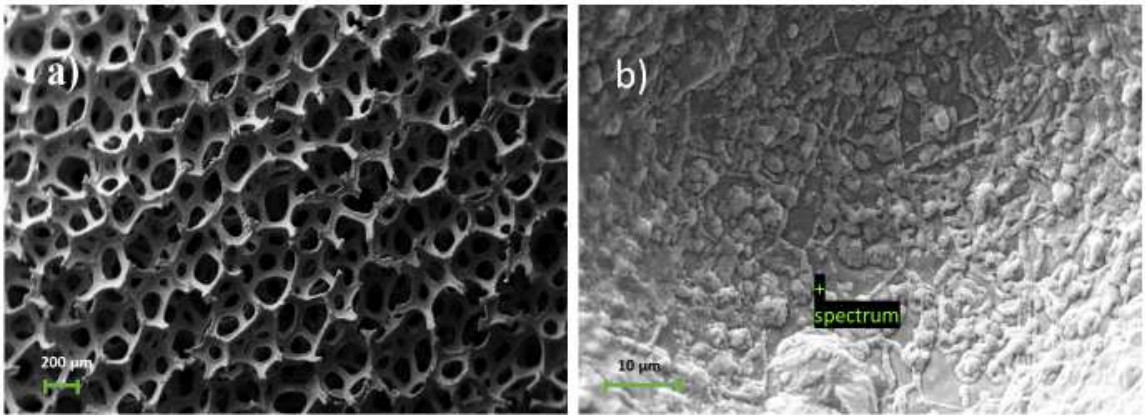

Figure 3.5: SEM images of Ni foam calcinated at 650°C at different magnification

Micro-Raman spectroscopy, Fig. 3.6, confirms the presence of metal oxides on the surface, with the presence of the same bands than in the spectra of previous foam. While in the diffraction pattern (Fig. 3.7) more intense NiO reflections than in the sample calcined at 500°C are recorded.

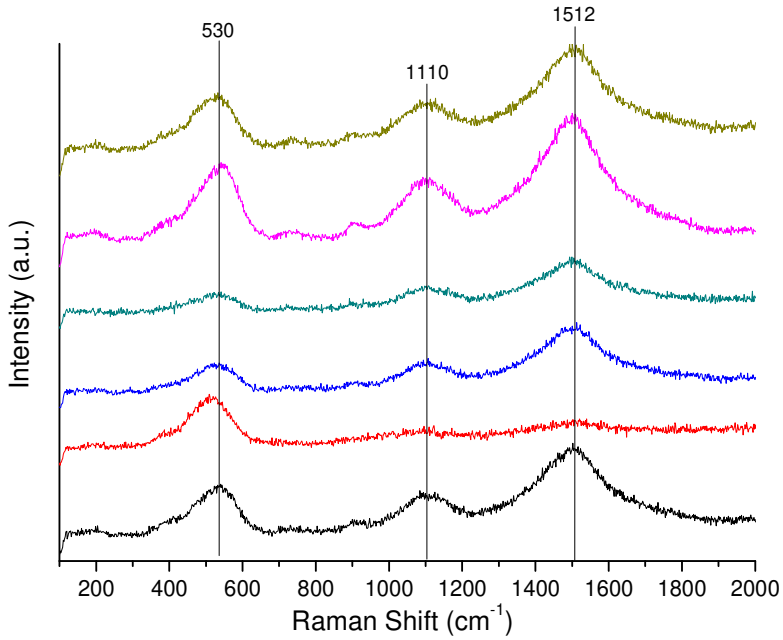

Figure 3.6: Raman spectra of a Ni foam calcined at 650°C

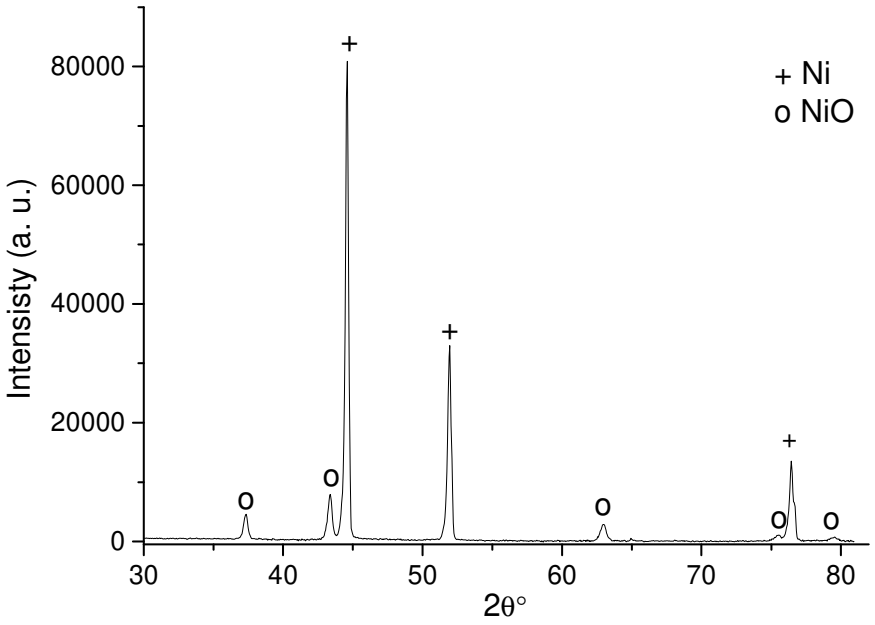

Figure 3.7: XDR pattern of a Ni foam calcinated at 650°C

SEM characterization of the foam, Fig. 3.8, after electrodeposition of $Ni(OH)_2$ shows the formation of a 3µm layer, this covers almost all the foam surface, though some cracks are

observed due to the drying process. It should be remarked that in some regions the thickness of the material reaches almost 7 µm.

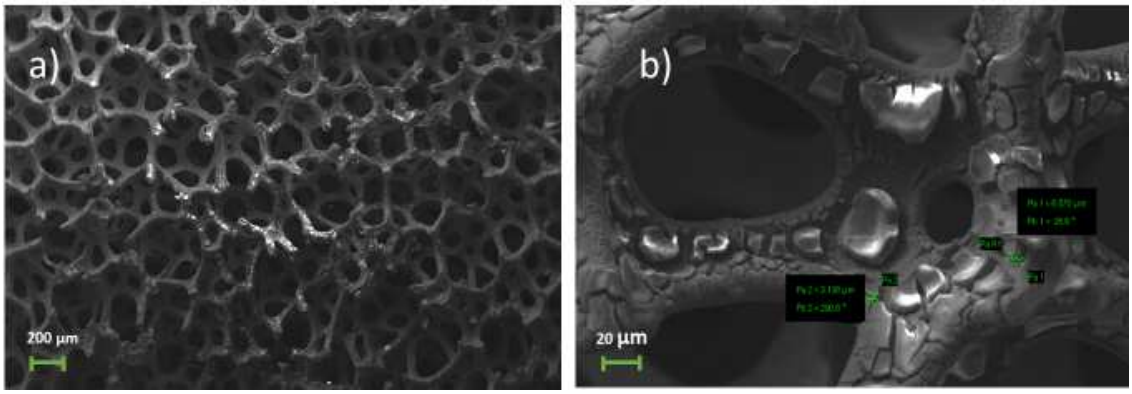

Figure 3.8: SEM images of $Ni(OH)_2$/Ni foam at different magnification

In the Raman spectra in Figure 3.9, the band at 1067 cm^{-1} is characteristic of the second order lattice mode of the α-$Ni(OH)_2$ phase, while the bands at 3438 and 3581 cm^{-1} are assigned to adsorbed H_2O, crystal defects, impurities, surface OH groups and the A_{1g} O–H stretching for both the α e β-$Ni(OH)_2$ phases [110].

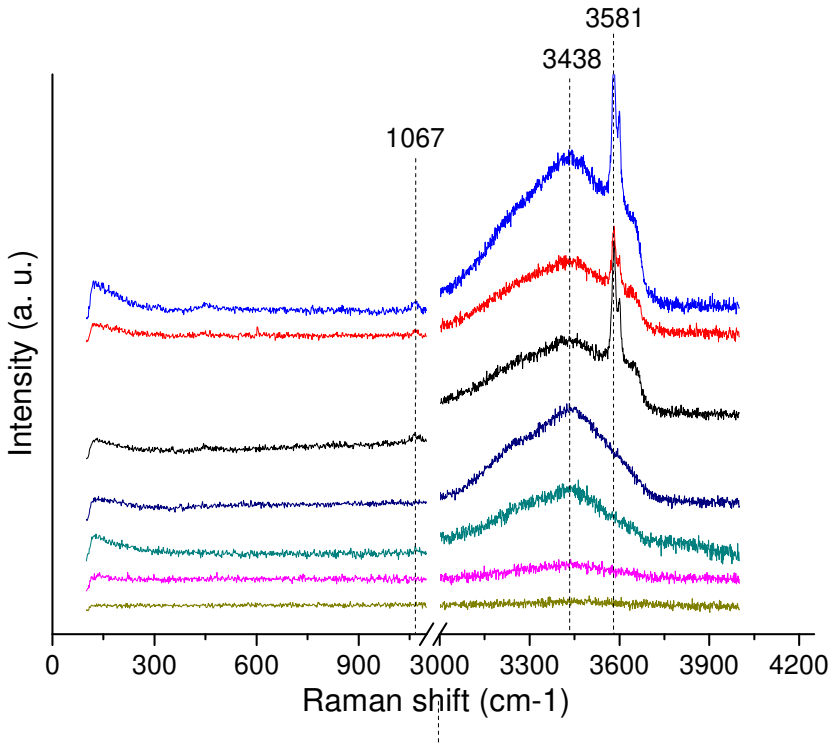

Figure 3.9: Raman spectra of a $Ni(OH)_2$/Ni foam

For this catalyst, diffraction lines associated with Ni hydroxide are not recorded, probably due to the poor crystallinity of the deposited material.

3.2 Electrochemical characterization of foams: cyclic voltammetry in NaOH and Glucose 10mM and 50mM

The cyclic voltammetry at the four different Ni foams (bare, after calcination at 500 and 650°C and $Ni(OH)_2$ deposition) are shown in Fig. 3.10-3.13. For the Ni bare and the calcined foams (Fig. 3.10-3.12) the current discharge is mainly due to the evolution of O_2, the onset for this process is recorded at about 0.5V vs SCE. However, a higher magnification of the plots reveals the presence of low intensity peaks at ca. 0.4V vs SCE, related to the Ni^{2+}/Ni^{3+} pair in basic conditions. The anodic peak represents the release of electrons, due to the electro-oxidation of $Ni(OH)_2$ to nickel oxyhydroxide (NiOOH) and the cathodic peak is associated with the inverse process in an alkaline environment [111]. The redox processes involving the Ni(II) and Ni(III) species are described by reactions 3.1, 3.2 [112]:

$$Ni(OH)_2 + OH^- \rightarrow NiOOH + H_2O + e^- \quad (3.1)$$

$$NiOOH + H_2O + e^- \rightarrow Ni(OH)_2 + OH^- \quad (3.2)$$

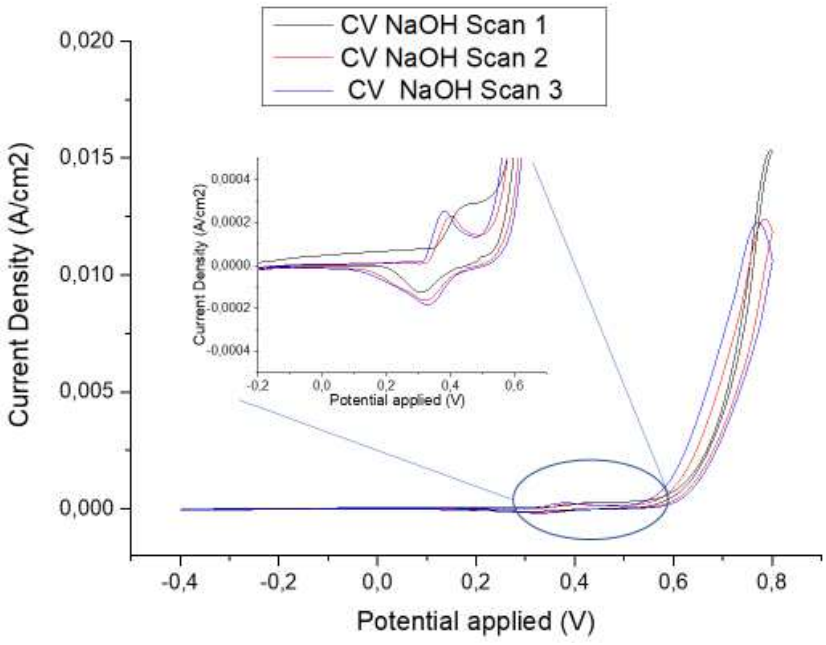

Figure 3.10: cyclic voltammetry for a Ni bare foam in a solution of 0.1M of NaOH; insert: magnification of the area between -0.2V and 0.6V vs SCE.

A maximum current density of 0.3 mA/cm^2 is recorded for the bare foam, moreover the peaks are slightly modified during the CV scans. In the first scan this peak is overlapped with the onset of the OER, while in the following scan it became sharper. In this case the transition from Ni(0) to Ni(II) does not take place via and electrochemical process but due to the passivation of Ni(0) in an alkaline environment, according to reaction 3.3 [93]:

$$Ni + 2OH^- \rightarrow Ni(OH)_2 + 2e^- \quad (3.3)$$

The low current density recorded for this step is probably due to the low amount of Ni hydroxide formed in this process. At higher potential it is shown an increase in the current density due to the OER, which reaches at 0.8V vs SCE a value of c.a. 13 mA/cm^2.

In the cyclic voltammetry at the Ni foam calcined at 500°C (fig. 3.11), the Ni^{2+}/Ni^{3+} pair is recorded at 0.4V vs SCE but with a lower current density than for the Ni bare foam. The peaks increase during the CVs. In addition, a small peak is observed at around -0.1V vs SCE. This foam shows a current density at the maximum of the OER that reaches 25 mA/cm^2, two times the value reached by the bare foam, this gives an indication of the activity of the two catalysts.

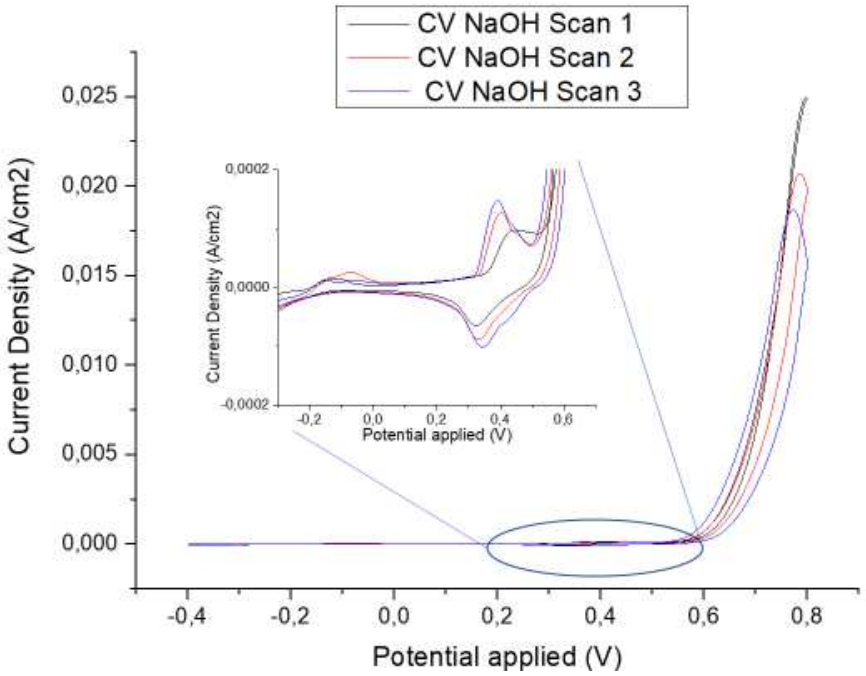

Figure 3.11: cyclic voltammetry for a Ni foam calcinated at 500°C in a solution of 0.1M of NaOH; insert: magnification of the area between -0.2V and 0.6V vs SCE.

The cyclic voltammetry at the Ni foam calcined at 650°C (Fig. 3.12) follows the same trend as above commented. Here the peak due to the redox pair Ni^{2+}/Ni^{3+} shows a maximum at around 0.4V vs SCE and a current density around 0.07 mA/cm^2, even lower than with the previous foams. The current density in the OER region shows a maximum of 14 mA/cm^2 almost the same value thanc for the other calcinated foam. The current density of the peak in the range between -0.2V and 0V increased compared to the foam calcined at lower temperature. The process is reversible, in fact we can observe a reduction peak that starts at -0.2V vs SCE and continues up to -0.4V vs SCE.

These peaks pair is not visible for Ni bare and $Ni(OH)_2$ foams, it is possible that it is related to a different electrochemical mechanism to form Ni hydroxide or other NiO species on calcined foams.

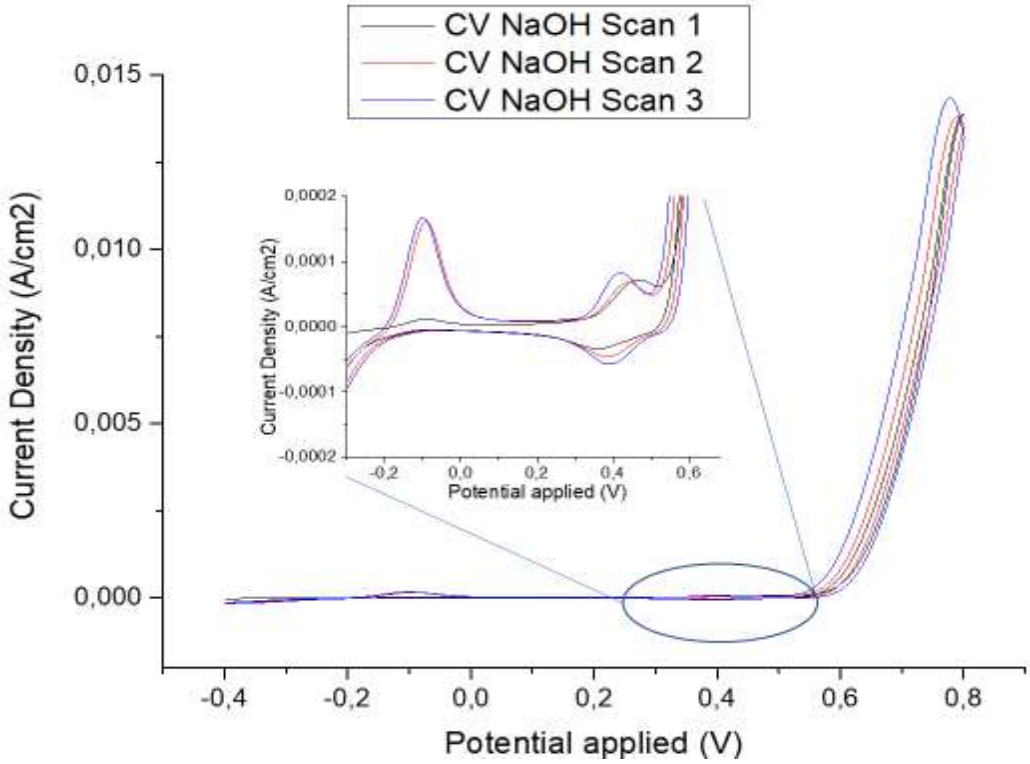

Figure 3.12: cyclic voltammetry for a Ni foam calcinated at 650°C in a solution of 0.1M of NaOH; insert: magnification of the area between -0.2V and 0.6V vs SCE.

In Figure 3.13 the cyclic voltammetry for the Ni deposited foam shows an anodic peak at around 0.45V with a current density of 15 mA/cm^2 due to the oxidation of $Ni(OH)_2$. This peak is more intense than for the previous foams. Furthermore, it is overlapped with the discharge of the OER, which at 0.8V reaches a maximum of 45 mA/cm^2, two times the value reached with the other foams. In the back scan, a cathodic peak is registered at around 0.3V with a current density of -10 mA/cm^2 due to the reduction of NiOOH.

Looking at the current density obtained with the deposited foam at 0.8V, it is possible to observe an increment with respect to the other type of foams. This result suggests that this foam is the most active for OER.

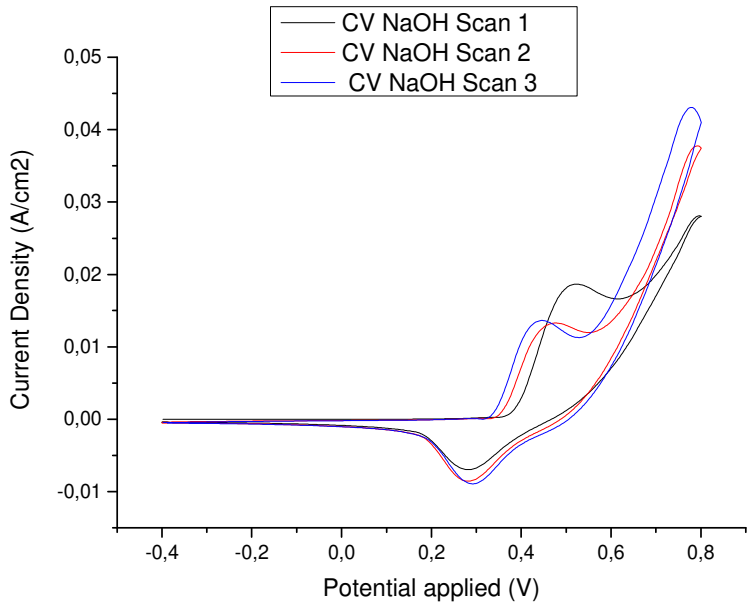

Figure 3.13: cyclic voltammetry for $Ni(OH)_2$/Ni foam in a solution of 0.1M of NaOH.

The cyclic voltammetries in basic solutions of D-glucose (10 mM and in 50 mM) are here discussed.

The shape of the curves recorded with a 10mM solution is rather similar for all the four electrocatalysts. The current starts to be recorded at around 0.2V vs SCE reaching a maximum at ca 0.4-0.6 V vs SCE, this peak is associated to the oxidation of the glucose in the solution and overlaps with the peak due to the OER. The position of the maximum and the current density depend on the type of catalyst.

The CV in glucose for the Ni bare foam, Fig. 3.14, shows the peak associated to the oxidation of glucose at around 0.5V vs SCE with a current density of 6 mA/cm^2. In the discharging scan a hysteresis phenomenon is observed, which is associated to the OH^- ions adsorbed on the interphase between the electrode and the electrolyte that are oxidised in the discharging part. This is due to the lower rate of the adsorption/desorption process of the OH^- ions on the surface of the electrode in comparison to the rate of the oxidation reaction [113]. Furthermore, it is noticeable that the oxidation of glucose continues in the reverse scan until the potential reaches 0,4 V vs SCE [114]. The absence of a cathodic peak in the discharging scan means that the oxidation of glucose is irreversible.

Increasing the concentration of glucose, Fig. 3.14b, the peak associated to the GOR shows an increment in current density respect to the CV at lower concentration, 10 mA/cm^2 vs 7 mA/cm^2 for the CV in 10 mM glucose. In addition, the peak associated to the glucose oxidation is shifted to more anodic potential. The current density in the range between 0.6V and 0.8V due to the OER is lower than in the CV at 10 mM due to the competition between oxidation of glucose and OER.

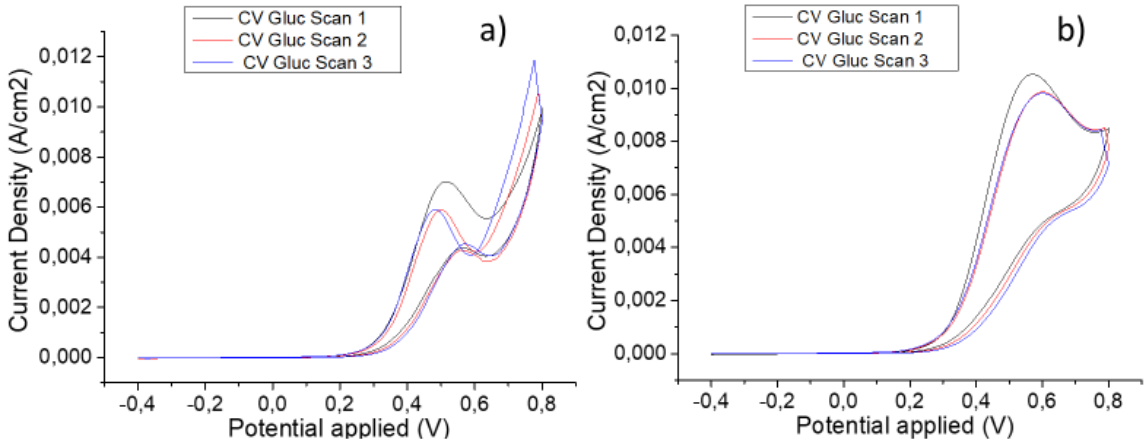

Figure 3.14: cyclic voltammetry for a Ni bare foam in a solution of a) 10 mM b) 50 mM of D-glucose

The CV in 10 mM glucose for the Ni foam calcinated at 500°C, Fig. 3.15a, shows the maximum current density due to the oxidation of glucose (7 mA/cm^2) at around 0.5V vs SCE, after that a plateau is recorded until 0.65V vs SCE. In this voltammetry the current density detected at the maximum of the OER is the highest in comparison to the other foams, 30 mA/cm^2. By increasing the concentration, it is registered an increasing of peak due to the GOR, as for the bare foam, and a lower current density value in the OER.

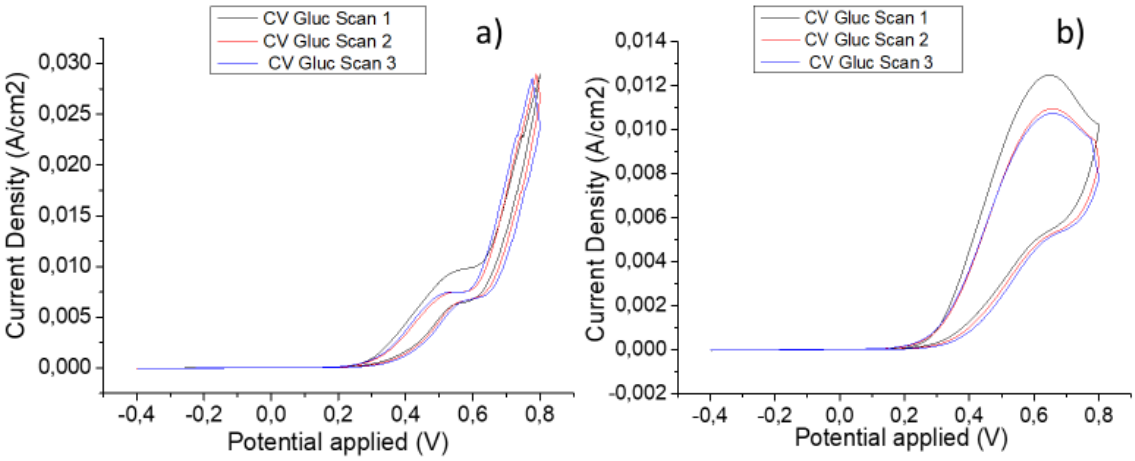

Figure 3.15: cyclic voltammetry for a Ni foam calcinated at 500°C in a solution of a) 10 mM b) 50 mM of D-glucose.

The CV in 10 mM glucose for the Ni foam calcinated at 650°C, Fig. 3.16a, the onset potential is similar to the previous calcinated foam but the plateau is not as defined as for the previous sample. The current density registered at 0.8V vs SCE is like the one for the Ni bare foam.

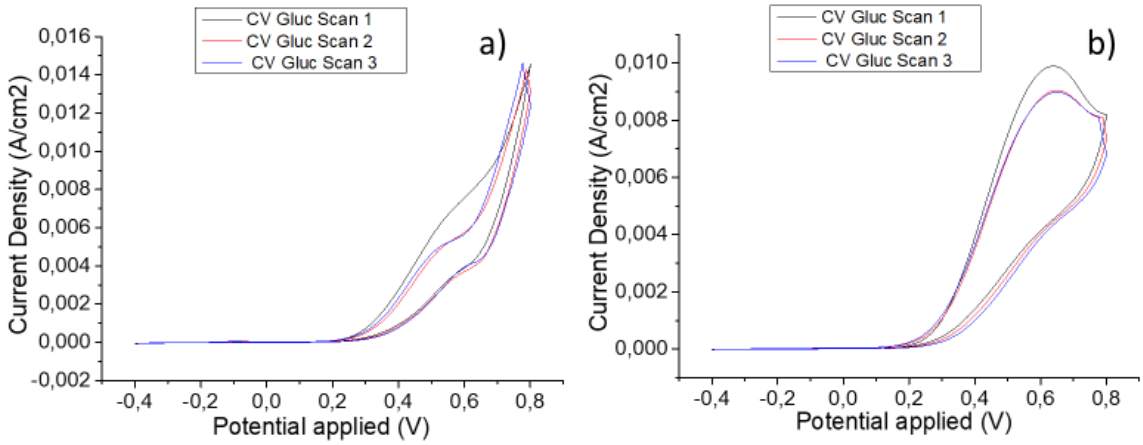

Figure 3.16: cyclic voltammetry for a Ni foam calcinated at 650°C in a solution of a) 10 mM b) 50 mM of D-glucose

The deposited Ni foam shows the highest current density for the peak associated to the glucose oxidation, Fig. 3.17a, around 14 mA/cm^2. This peak is shifted to higher potential, 0.55V vs SCE, in respect to the other foams. In this sample, it is possible to observe the peak in the discharging scan (around 0.3V vs SCE) due to the reduction of Ni(III) species to Ni(II), previously observed in the CV in NaOH solution. This peak is not visible with

high concentration of glucose, Figure 3.17b. The reason could be associated to the fact that at a higher concentration of glucose all the Ni3+ species are involved in the oxidation of the organic molecule, and therefore are reduced, while at lower concentration of glucose, some Ni3+ species remains and they are reduced in the back scan.. In the solution at higher concentration, figure 3.17b, the currents evolved the GOR region remain unchanged while as expected the OER region shows a decrease in current density in respect to the one in Figure 3.17a.

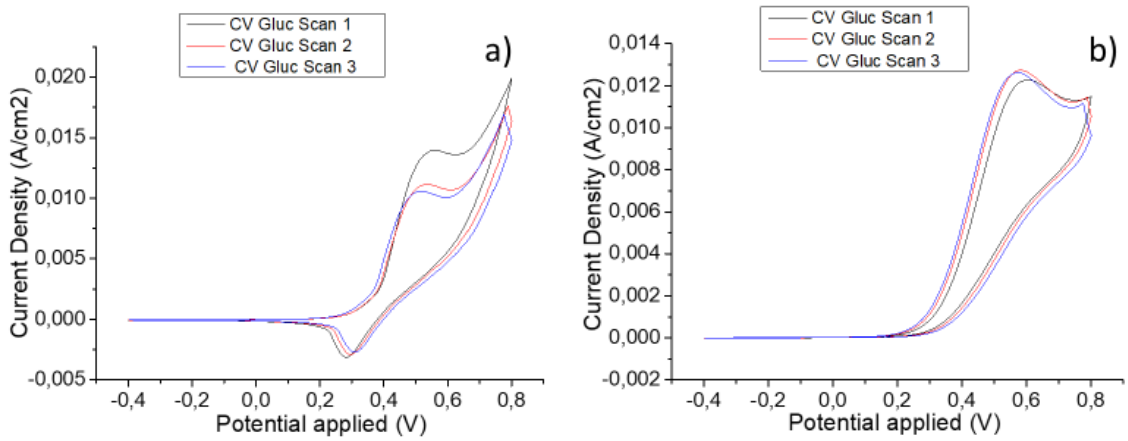

Figure 3.17: cyclic voltammetry for $Ni(OH)_2$/Ni foam in a solution of a) 10 mM and b) 50 mM of D-glucose.

3.3 Electrochemical oxidation of glucose

In this section the electrochemical tests performed to quantify the catalytic activity of the foam electrodes in terms of conversion of glucose, selectivity and faradic efficiency are presented.

Firstly, the effect of the potential on the activity is investigated, chronoamperometries are performed at selected potentials over the Ni bare foam. From the cyclic voltammetry we defined that the GOR for all the catalysts starts around 0.4 V and has the maximum around 0.5-0,6V vs SCE. For this reason we decided to test three potentials, 0.6V, 0.7V and 0.8V in 25mL solution of glucose 50mM accumulating a charge of 241.48C, considering the charge needed to reach the total conversion of the glucose to GO.

The choice of the high concentration was made in order to minimize the influence due to the OER.

The faradic efficiency for gluconic acid was calculated considering a redox process involving two electrons, while for glucaric acid was considered the total transfer of 6 e^-: $2e^-$ to give GO and others $4e^-$ for the subsequent oxidation to give GA.
The process follows the course indicated in the following reactions (3.4 – 3.5):

$$C_6H_{12}O_6 + 2OH^- \rightarrow C_6H_{12}O_7 + H_2O + 2e^- \quad (3.4)$$

$$C_6H_{12}O_7 + 4OH^- \rightarrow C_6H_{10}O_8 + 3H_2O + 4e^- \quad (3.5)$$

The results from the analysis are settled in table for an easily comprehension. From the data in table 3.1 emerges that the test carried out with 0.8V shows the best results in terms of: glucose conversion, 65% vs 52% and 54% of the 0.6V and the 0.7V tests respectively; selectivity toward GO, 60% vs 18% and 46%; FE toward GO and GA, that reach 39% and 7% respectively. For this reason all the cyclic amperometry in the next session have been carried out with this potential.

Table 3.1: test performed at different potential on the Ni bare foam

Potential (V)	**Glucose conversion (%)**	**Selectivity to GO (%)**	**Selectivity to GA (%)**	**FE_{GO} (%)**	**FE_{GA} (%)**
0.6	52	18	2	10	3
0.7	54	46	4	25	6
0.8	65	60	3	39	7

3.3.1 Catalytic test in a solution of glucose 10mM

The foams were tested in a 25 mL solution of glucose 10mM until reaching a charge to oxidize all the glucose to gluconic acid (48C).
The Ni calcined 500°C foam, Fig. 3.18, exhibits the best results in terms of glucose conversion (47%), while the Ni bare foam and the Ni foam calcinated at 650°C show glucose conversions of 37% and 33%, respectively.
The deposited foam is confirmed as the less active toward the glucose conversion, 15%.

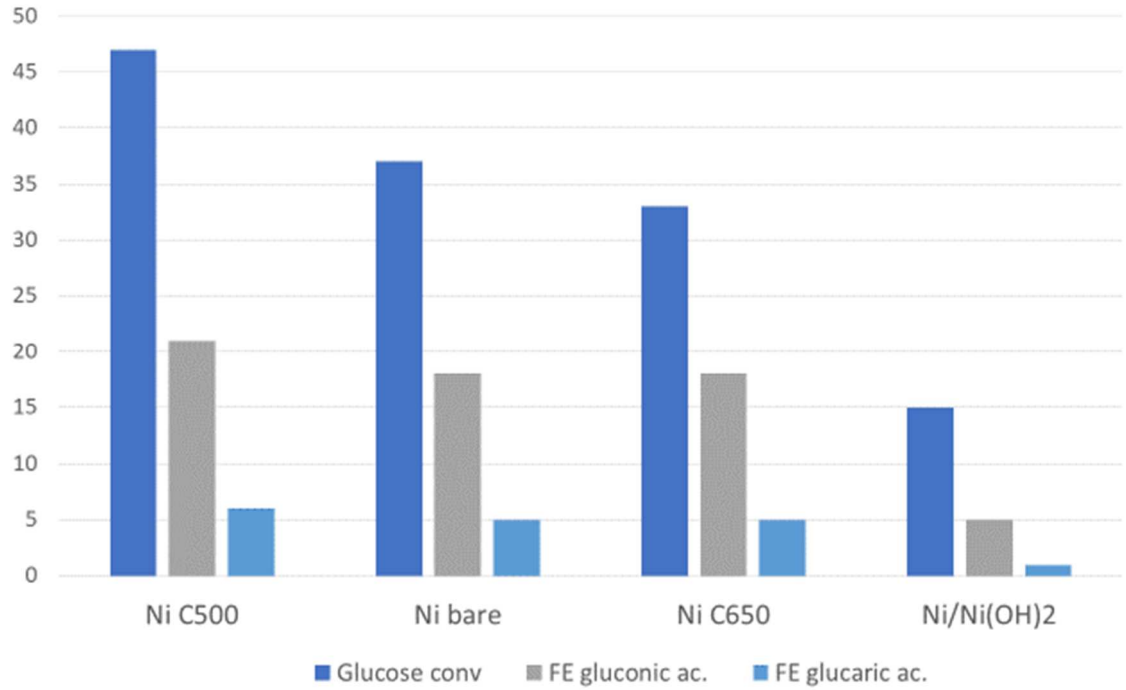

Figure 3.18: Comparison of the results of glucose conversion and FE in gluconic and glucaric acid between the different foams.

In the Figure 3.19 the selectivity of the catalysts for all the reaction products is shown. As expected, all the catalyst present a selectivity toward GO greater that the one toward GA. Moreover, it can be observed that the Ni foam calcinated at 650°C shows the best selectivity toward both the desired products, 51% to GO and 4% to GA probably due to the amount of Ni oxides present on the surface of the foam; both the Ni bare foam and the Ni foam calcinated at 500°C show good results in term of selectivity toward GO, respectively 47% and 44%. The other products formed are due to further reaction of oxidation on the products, the most abundant for both the four foam are: formic acid, gliceric acid and oxalic acid.

The deposited foam exhibits the lowest selectivity toward GO, 33%, and GA, 3%, probably due to the formation of further oxidized products. Indeed from the Fig.3.19 it is possible to observe that the deposited foam shows higher percentages of undesirable products with respect to the other foams in particular formic acid (28%), -keto-3-deoxygluconate (2KDG) (8%) and oxalic acid (6%).

In terms of FE the Ni foam calcinated at 500°C shows a FE to GO (21%) and FE to GA (6%) while the bare foam and the calcinated at 650°C show the same FE for both the products, 18% to GO and 5% to GA; anyway as expected the deposited foam show the worst result in terms of FE, 5% to GO and 1% to GA.

As it is possible to observe, only with the deposited foam it is reached 100% selectivity toward products. This is because at the moment there are some peaks of the HPLC chromatograms not identified yet and also for the total oxidation of glucose to give CO_2.

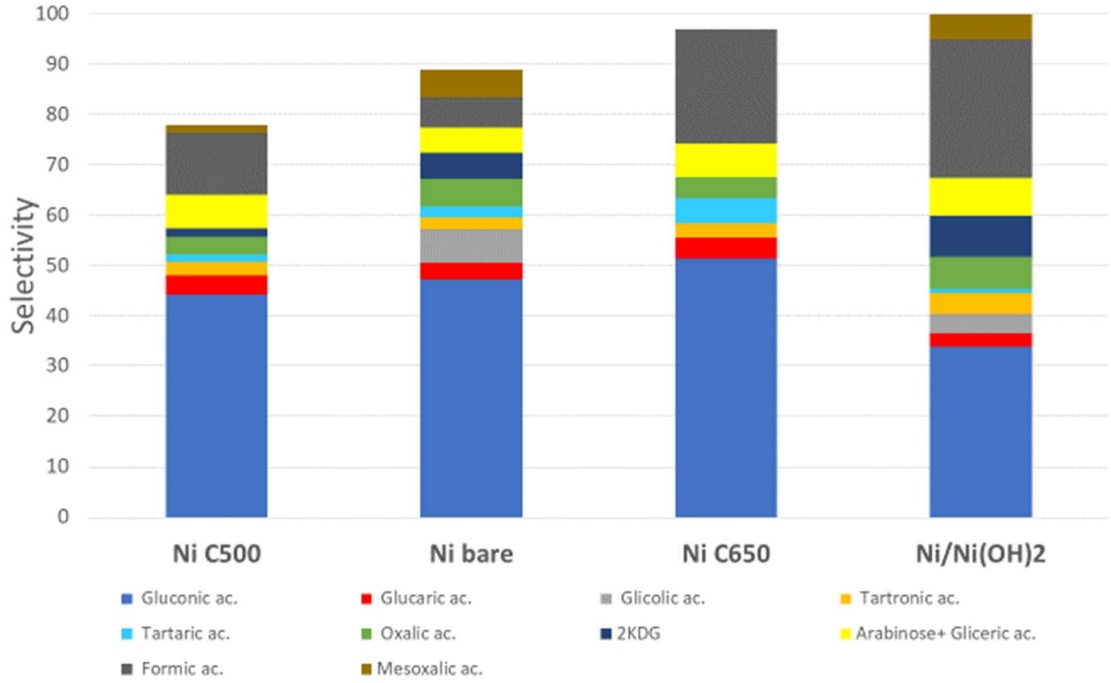

Figure 3.19: selectivity of the different foams toward the products.

3.3.2 Cyclic voltammetry after catalytic tests

Both the CV in NaOH and glucose are performed after the CA to understand if the catalysts change due to the reaction.

In this section, the results obtained with the Ni foam calcinated at 500°C will be presented as an example, since we found out the same trend for both the Ni bare and the Ni calcinated at 650°C.

In Figure 3.20 the third scans of the cyclic voltammetry before (CV1) and after (CV2) the reaction are shown. The peaks associated to Ni redox pair in both the charging and discharging scan are more intense after reaction at 0.8 V, reaching a value of 30 mA/cm^2. Moreover, an increment of the current density is also registered in OER potential range, i.e. between 0.6V and 0.8V. Thus, the catalyst may be activated during the reaction probably due to changes in the morphology of the electrode surface.

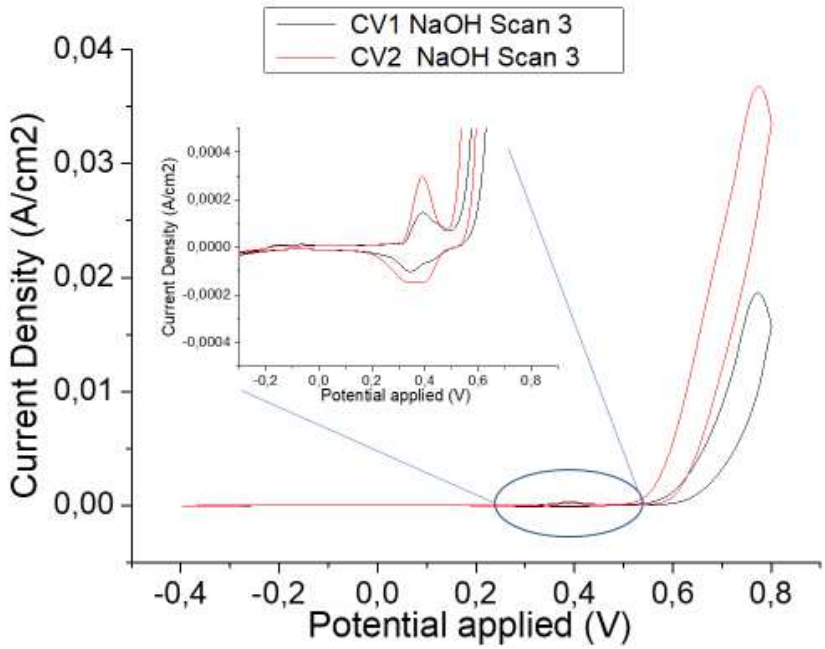

Figure 3.20: cyclic voltammetry CV1 before and CV2 after the reaction for the Ni foam calcinated at 500°C in NaOH 0.1M solution.

In the cyclic voltammetry in glucose 10mM, Fig. 3.21, there are not noticeable differences in the GOR region between the CVs before and after reaction for the Ni foam calcinated at 500°C, however, an increment in current density is registered in the OER region showing that, as before the foam may have been activated.

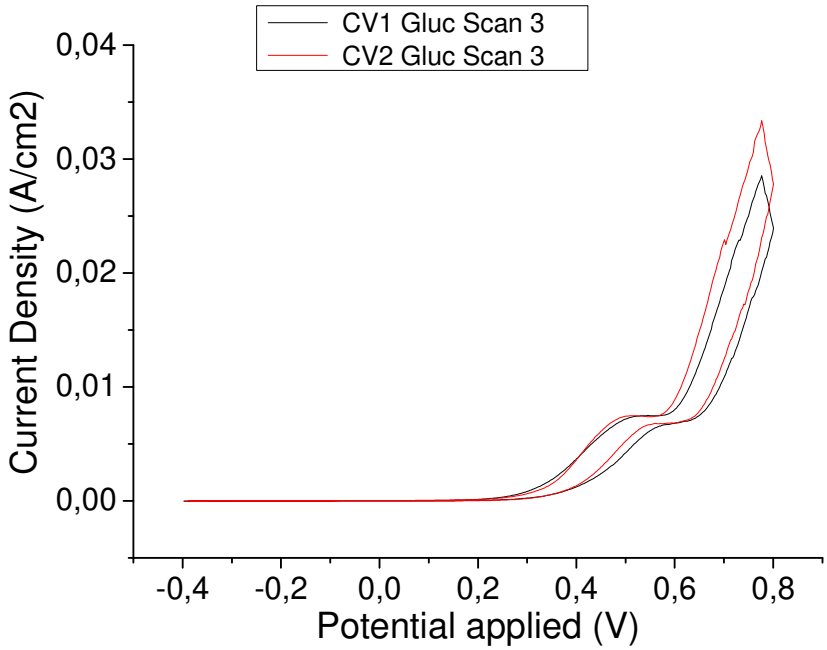

Figure 3.21: cyclic voltammetry CV1 before and CV2 after the reaction for the Ni foam calcinated at 500°C in a 10 mM glucose solution.

For the deposited Ni foam, Fig 3.22, after the reaction a lower density current is registered in the voltammogram in NaOH than that before reaction. This behaviour is related to the leaching of the deposited material on the surface during the catalytic cycle. Indeed after reaction a green solid, probably $Ni(OH)_2$, is observed in the reaction solution.

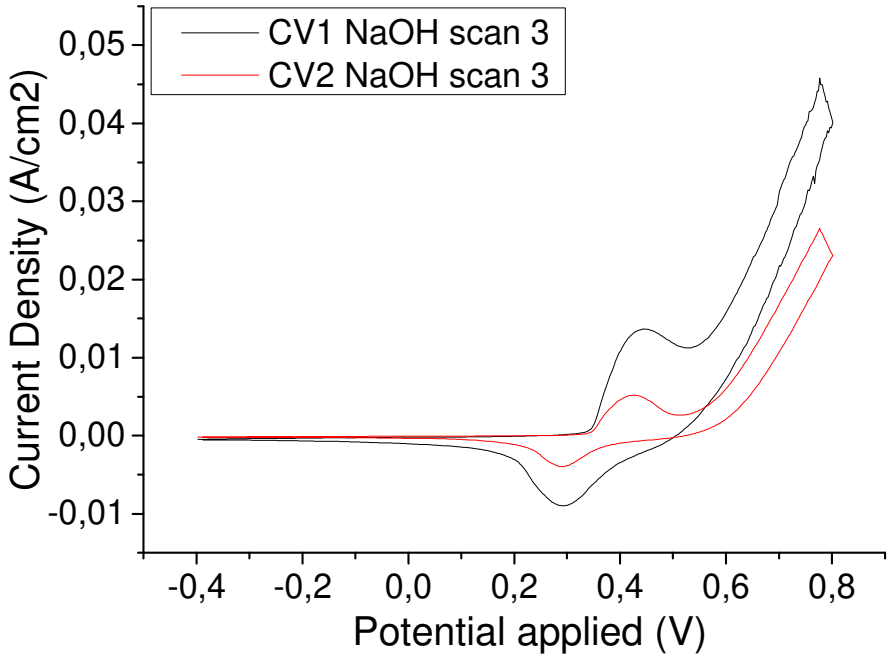

Figure 3.22: cyclic voltammetry CV1 before and CV2 after reaction for $Ni(OH)_2$/Ni foam in a 0.1M NaOH solution.

In the Figure 3.23 the deposited foam shows a decrease in the current density in the GOR region after the reaction in a 10 mM glucose, as expected, due to the leaching of the deposited material, while in the OER region an increment of the current density is observed. The lower activity of the foam toward glucose conversion results in a lower competition between the GOR and the OER.

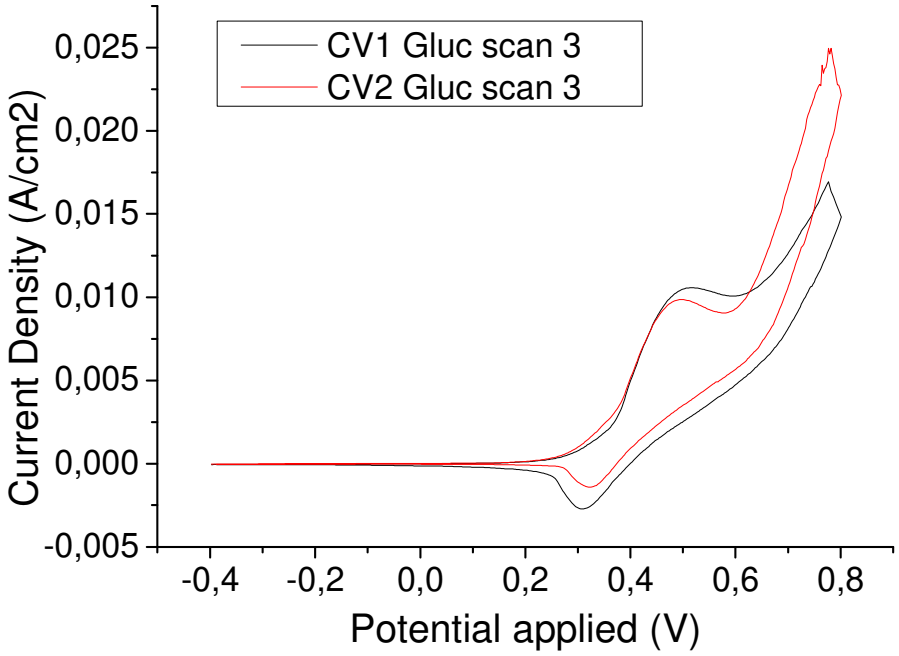

Figure 3.23: cyclic voltammetry CV1 before and CV2 after reaction for $Ni(OH)_2$/Ni foam in a 10 mM glucose solution.

3.4 Effect of the charge on electroactivity

To understand the evolution of the reaction with the collected charge, namely with the reaction time, tests are run by collecting lower charges in the 10 mM glucose solution with Ni foam calcinated at 500 °C, due to the its better performance. It should be remarked that due to the high reproducibility of the tests, CVs in both NaOH and glucose are similar to those reported in the previous section, therefore they are not included here.

The conversion of glucose increases with the increasing accumulated charge; however it is very low at 12C ca. 6% and 12% at 24C. Evaluating the data in Figure 3.24 it is possible to recognise that at the beginning of the reaction the selectivity is mainly towards the formation of GO, reaching a selectivity as high as 76% with only minor amounts of oxalic and formic acid. Increasing the charge collected to 24C, and therefore the reaction time, ,the selectivity toward the GO decrease, with a simultaneous formation of other oxidation products and also consecutive oxidation products of GO, to form other molecules with a lower number of Carbon atoms, such as oxalic acid and formic acid.

In the first two tests any traces of GA was not detected while in the tests at 48C a selectivity of 4% was registered toward the GA.

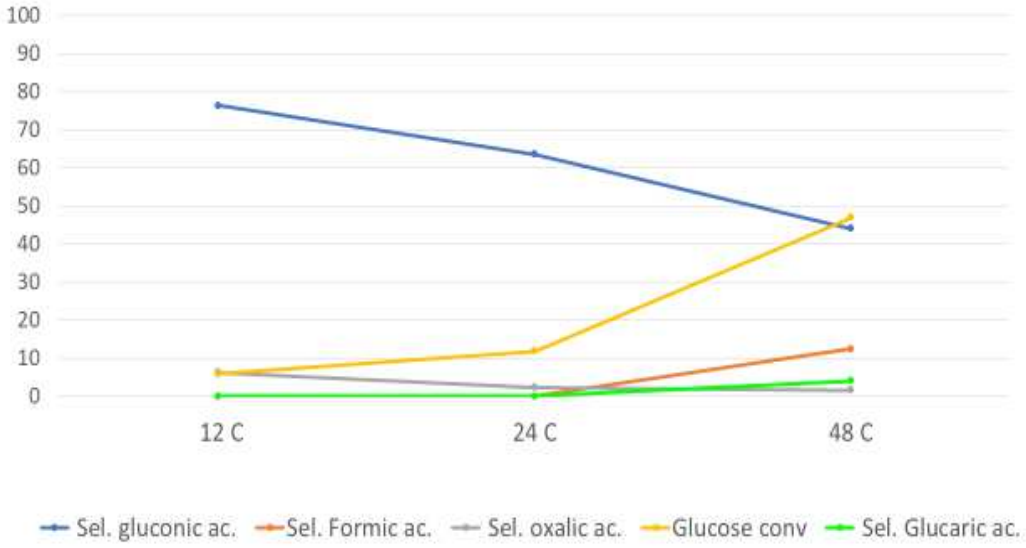

Figure 3.24: electroactivity of Ni foam calcinated at 500°C at different accumulated charge.

3.5 Effect of glucose concentration

3.5.1 Electrochemical tests with 50 mM glucose solution

In Figure 3.25 the results of conversion and FE are shown with the 50 mM glucose solution.

As expected by looking to the CV, increasing the concentration of glucose, an increase in the conversion is observed. The catalyst that shows the best conversion is the Ni foam calcinated at 650°C (55%), but the difference with Ni bare and Ni C500 is not very high (52-53%) and these similarities is also reflected in the FE.

As observed in the tests at lower concentration, the deposited foam shows the worst results in terms of FE toward the GO while the conversion to glucose (46%) does not follow the same trend showing a great increment.

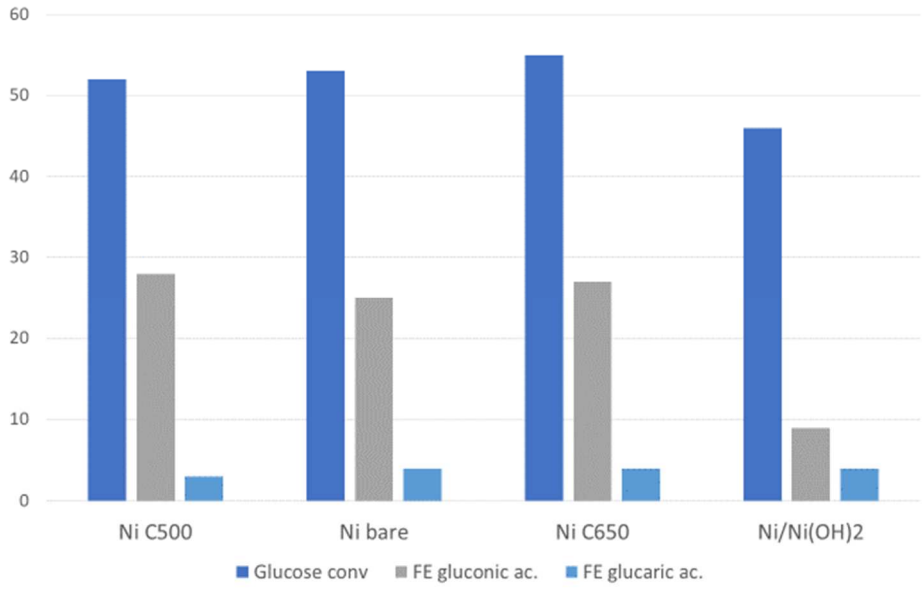

Figure 3.25: electroactivity of the different foams with 50 mM glucose solution

The trend in selectivities obtained with the 50 mM glucose solution is rather similar than that with a 10 mM solution Figure 3.26. However, an increase in selectivity of 9% is observed for the Ni foam calcinated at 500°C for the more concentrated solution, while the Ni foam calcinated at 650°C shows a decrease of 3% in selectivity. On the other hand, the deposited foam is the least selective toward GO and it suffers from the greatest decrease with respect to the tests at lower concentration, 18% vs the 34% of the 10 mM tests.

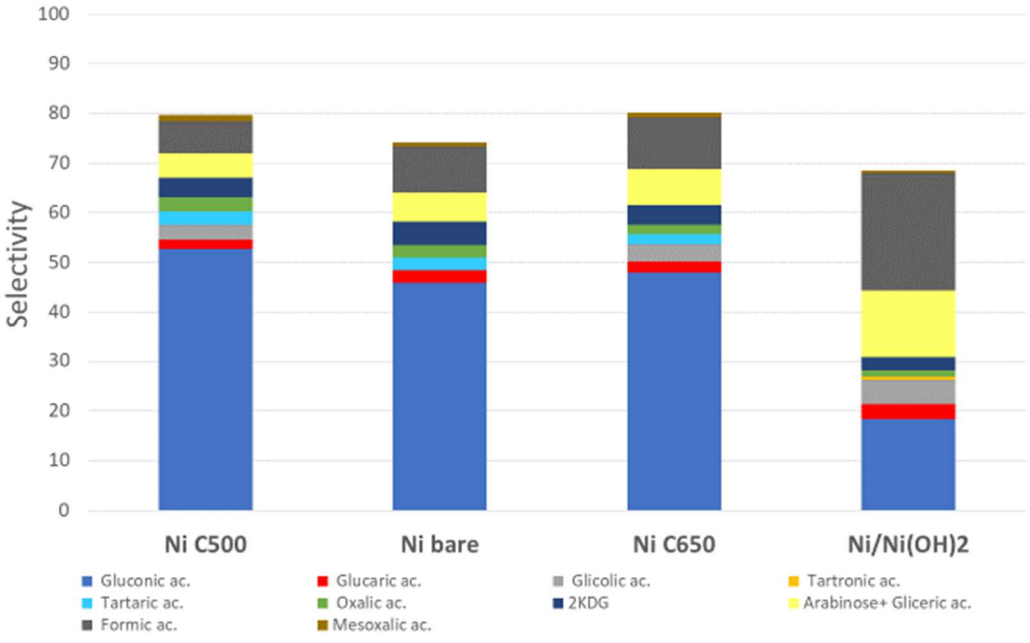

Figure 3.26: selectivity of the different foams toward the products

CVs in NaOH before and after reaction are similar, Fig. 3.27, therefore the CVs in NaOH are not shown here. An exception is made for the deposited foam that show a decrease in current density of the peak associated to the Ni redox couple; this is due to the leaching of the deposited material on the support.

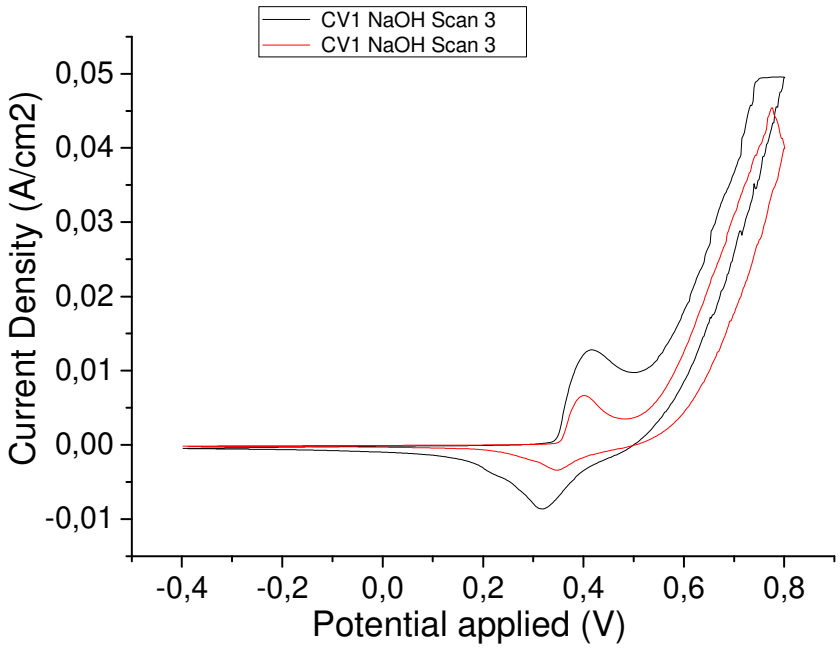

Figure 3.27: cyclic voltammetry in NaOH solution CV1 before and CV2 after reaction: $Ni(OH)_2$/Ni foam.

In Figure 3.28, CVs before (CV1) and after (CV2) reactions in the solution of glucose 50 mM are shown. The current due to GOR slightly increases after reaction, thus suggesting that the surface of the electrode is modified during electrocatalytic tests; however, this modification seems to only alter the activity in GOR rather in OER.

Unlike the reaction at lower concentration, the deposited foam does not show a decrease in current density after reaction.

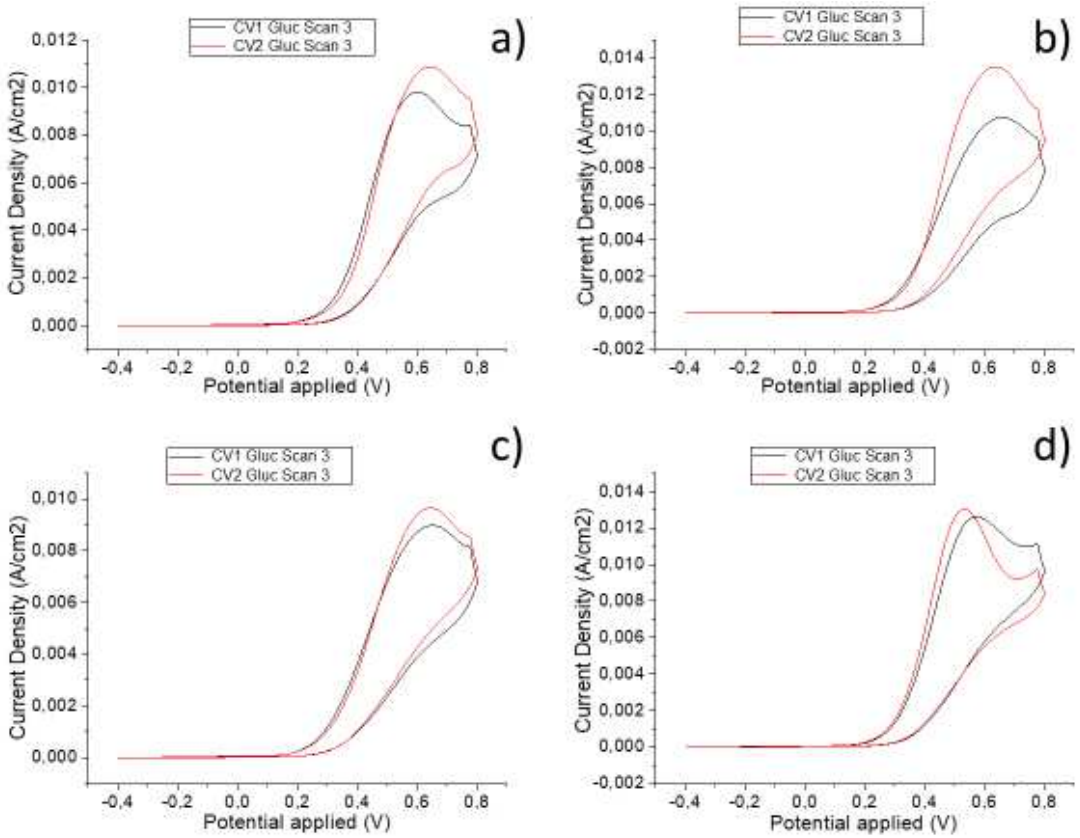

Figure 3.28: cyclic voltammetry in glucose solution CV1 before and CV2 after reaction: a) Ni bare foam, b) Ni foam calcinated at 500°C, c) Ni foam calcinated at 650°C, d) $Ni(OH)_2$/Ni foam.

3.5.2 Electrochemical tests with 100mM glucose solution

In order to evaluate the effect of a higher glucose concentration on catalytic activity, the Ni foam calcinated at 500°C is tested with a 100 mM glucose solution.

As above reported the voltammogram in NaOH is not reported due to the reproducible results.

The CVs in glucose for both the three tests performed at different concentration are shown in in Figure 3.29. As expected, increasing the concentration of glucose the competition with the OER decreases, as a matter of fact an increment in the peak intensity related to the GOR is registered, c.a. 6mA/cm^2 (black), 8 mA/cm^2 (red) and 10mA/cm^2 (blue); moreover a shift of the peak toward lower potential is observed at higher concentration. While the currents recorded in the OER region decrease. The higher glucose concentration may saturate the active sites for the OER.

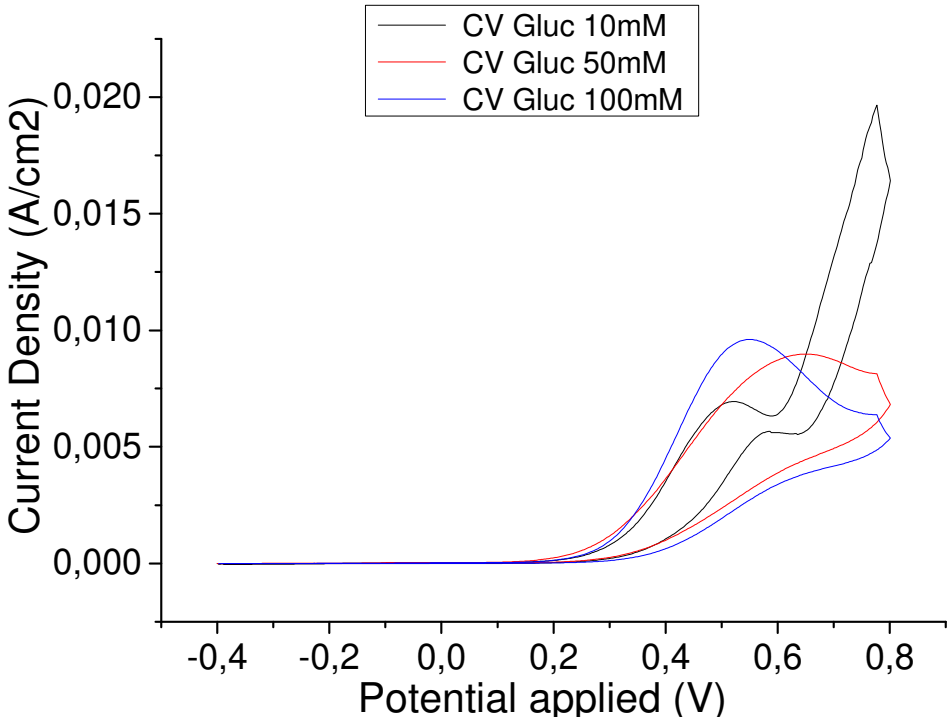

Figure 3.29: cyclic voltammetry of the Ni foam calcinated at 500°C in a solution of glucose of: 10 mM (black), 50mM (red) and 100 mM (blue)

The catalytic test was performed at the same temperature of the previous tests; the theoretic charge that should be accumulated is 482.96 C but due to the low time availability the reaction was stopped at 350 C.

In Figure 3.30, the conversion of glucose achieved is 45 % and the selectivity in GO of around 43 % is obtained, in the range of selectivities reported for the lower concentrated solutions; as in the previous tests at lower concentration there is the presence of side-products, the more abundant as the formic acid and 2KDG with selectivities of 9% and 5% respectively. However, it should be remarked that considering results in previous sections, if the charge accumulated reaches the theoretical value (ca. 483 C) a higher glucose conversion and a lower GO selectivities will be expected.

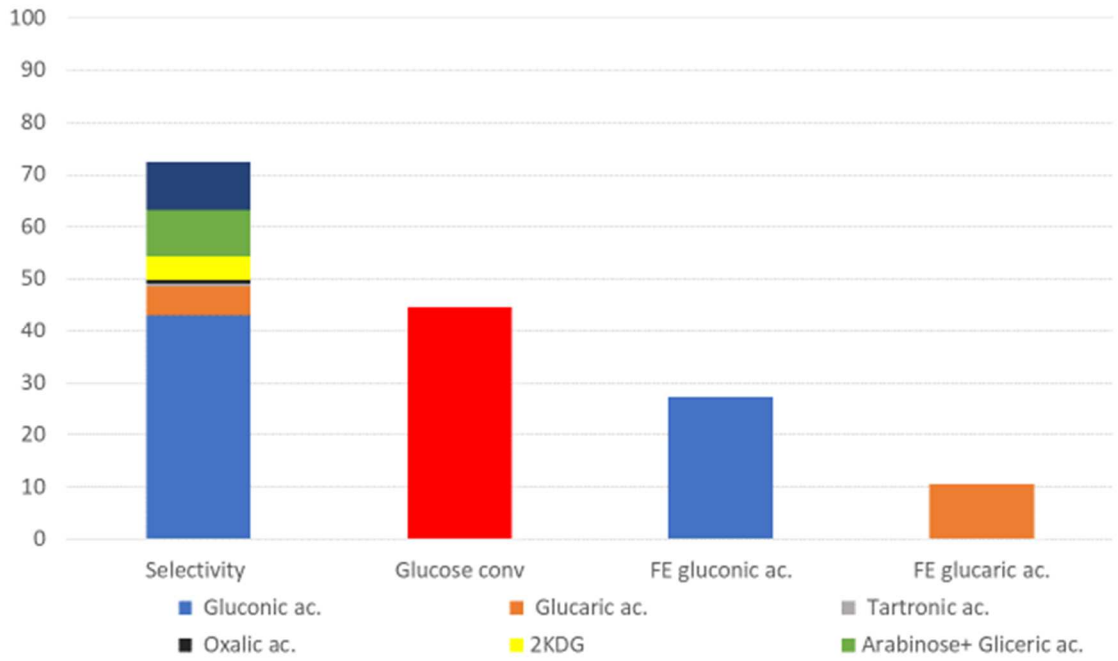

Figure 3.30: electroactivity of Ni foam calcinated at 500°C, with 100mM glucose solution.

The FE for both the gluconic and glucaric acid follow the same trend observed in the previous test, as a matter of fact the glucose conversion is c.a. 45% similar to the test at 10mM, 46%, and slightly lower than the test at 50mM, 51%.

Moreover the FE toward the GO shows a increment as the concentration of glucose increase: 22% in 10mM, 25% in 50mM and 27% in 100mM.

The cyclic voltammetry after the reaction of the Ni foam calcinated at 500°C does not show any noticeable differences, as it is possible to observe in Figure 3.31, the shapes of the voltammograms and the currents evolved before (CV1) and after (CV2) the reaction are very similar.

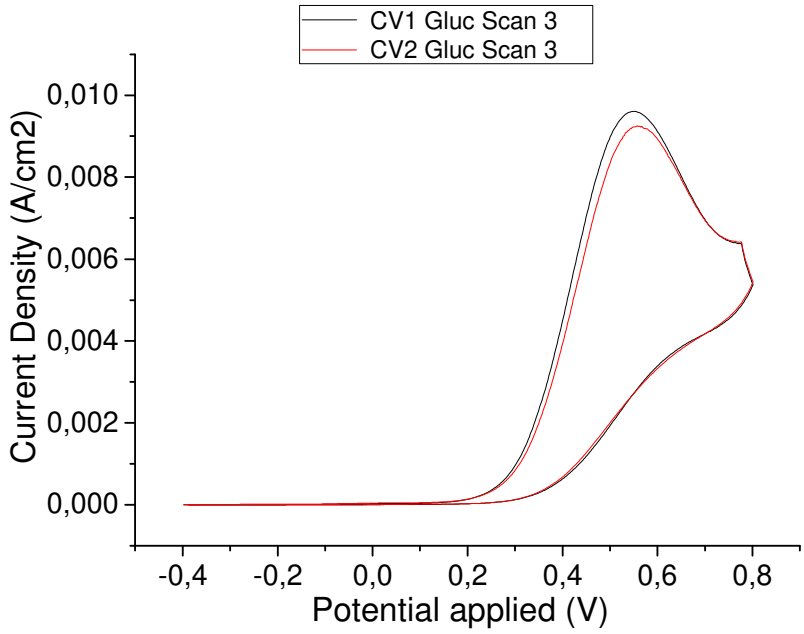

Figure 3.31: cyclic voltammetry CV1 before and CV2 after reaction for the Ni foam calcinated at 500°C in a solution of glucose 100 mM.

3.6 Characterization after reaction

In this following section, representative characterization results of the foams after reaction will be shown. There are not any remarkable difference in the foams depending on the concentration of the glucose solution.

SEM images of the bare Ni foams and foams calcined at 500 and 650°C, Fig. 3.32, show that there are not any large change of the surface during the reaction, despite the modification in the conversion reported in the previous sections. On the other hand, for the foam coated with $Ni(OH)_2$ the detachment of a considerable amount coating is observed, in agreement with the green deposits observed in the bottom of the electrochemical cell after tests, as above commented.

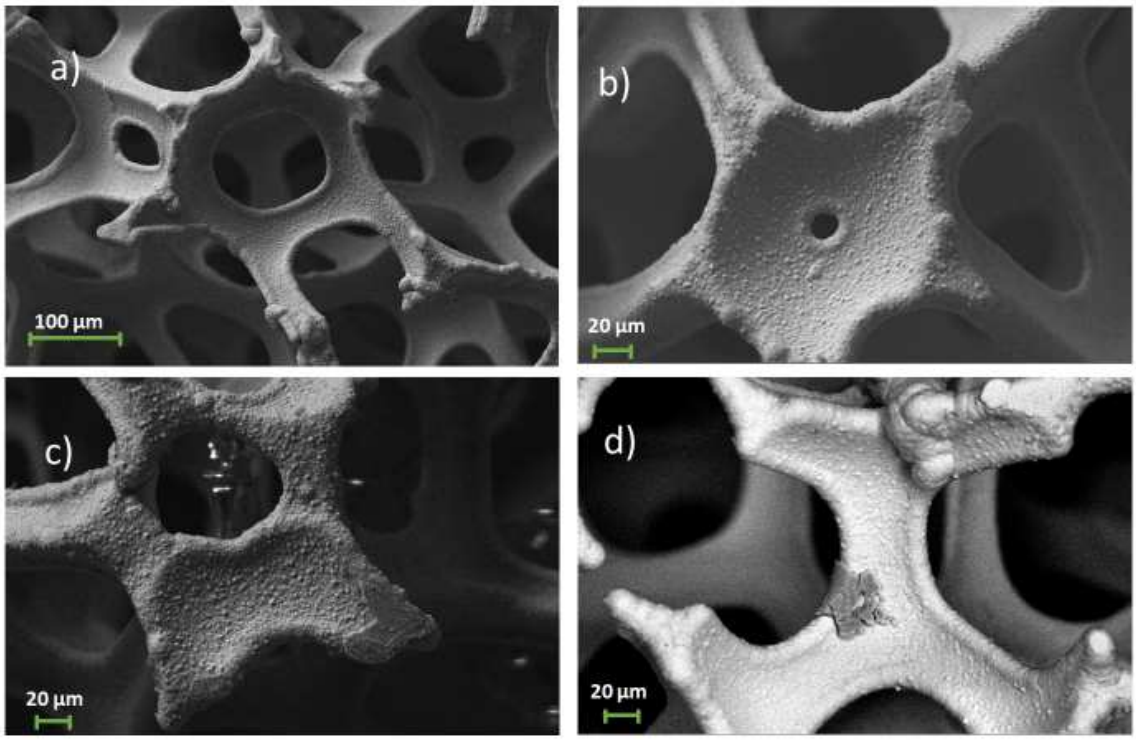

Figure 3.32: SEM images of Ni foams after reaction, a) Ni bare foam, b) Ni foam calcinated at 500°C, c) Ni foam calcinated at 650°C and d) $Ni(OH)_2$/Ni foam.

Micro-Raman spectra in the still coated regions confirmed the presence of Ni(OH)2, Fig. 3.33. Two low intensity peaks, one at 3582 cm^{-1} associated to a the disordered O-H stretching mode of the β-$Ni(OH)_2$ and the other at 3646 cm^{-1} associated to A_{2u} (LO) O-H stretching of the β-$Ni(OH)_2$ are shown.

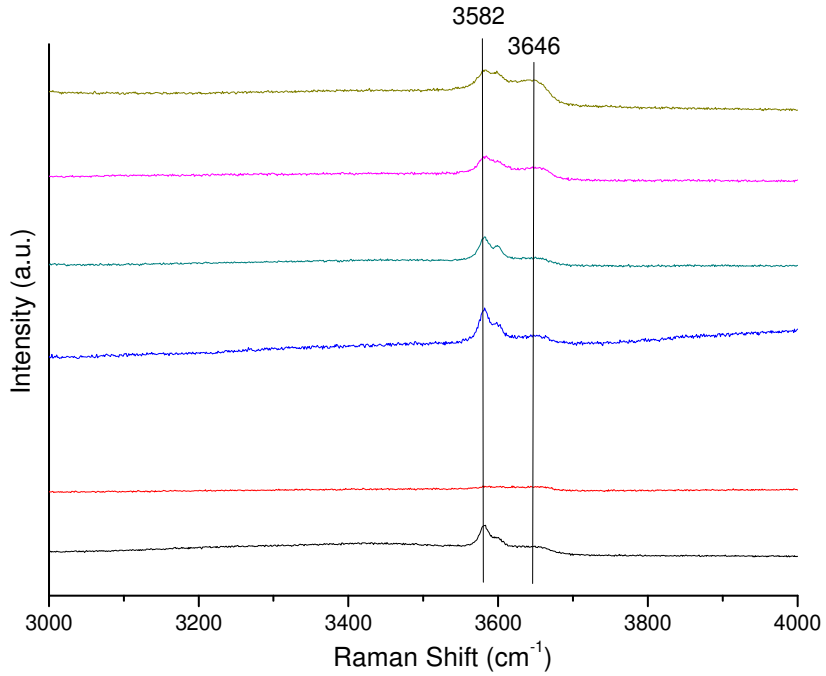

Figure 3.33: Raman spectra of the $Ni(OH)_2$/Ni foam after reaction.

The Raman spectra for the other foams are not showed because they do not present any detectable difference from the spectra before reaction.

Conclusions

The electrocatalytic properties of four Ni based metal foams towards the electrochemical selective glucose conversion to obtain gluconic (GO) and glucaric acid (GA) were investigated in this work.

The CVs in 1M NaOH solution showed that all the foams were active for the evolution of O_2. Only the Ni foam coated by $Ni(OH)_2$ showed an intense pair of peaks due to the transition between Ni hydroxide to oxyhydroxide, which are considered as active species for glucose oxidation. However, in CVs performed in a solution of glucose all the four electrocatalyst showed a good activity towards the glucose oxidation reaction, represented by a peak in the range between 0.4 and 0.6V vs SCE. Differences were observed in the CVs with the increase in the concentration from 10mM to 50mM, showing an increase of the peak intensity and a shift towards more anodic potential.

The electrocatalytic tests revealed that conversion and selectivity increased with the applied anodic potential, and 0.8V was the best potential in terms of selectivity towards the desired reaction, obtaining a glucose conversion of about 5% with GO selectivity of about 60%.

The study on the effect of the charge applied on the electroactivity revealed that, as expected, the glucose conversion increased with increasing the accumulated charge, while the selectivity towards GO decreased due to the simultaneous formation of other oxidation products such as formic acid, 2KDG and oxalic acid.

Tests performed to evaluate the effect of the concentration of glucose on the electrocatalytic activity showed that with increasing the concentration the competition with OER decreased resulting in a higher glucose conversion. However, the selectivity to side products increased, resulting in a decrease of the GO and GA selectivity.

The electrocatalytic tests showed that all four foams were active toward the GOR but only the Ni bare and especially the calcined foams showed a good selectivity toward the desired products. On the contrary for the deposited foam the selectivity in side products increased.

These results confirm the great potentiality of the Ni foams as the electrocatalysts for the glucose selective oxidation to GO, further studies are needed in order to optimize the reaction conditions to achieve better results.

Bibliography

[1] IEA, "CO2 Emissions from Fuel Combustion Highlights 2018," 2018. [Online]. Available: https://www.iea.org/publications/freepublications/publication/CO2EmissionsfromFuelCombustionHighlights2018.pdf.

[2] "ecotricity-when will fossil fuels run out," [Online]. Available: https://www.ecotricity.co.uk/our-green-energy/energy-independence/the-end-of-fossil-fuels.

[3] F. Trifirò and F. Trifirò, "Introduzione," in *La chimica in soccorso dell'umanità*, Bologna, 2018, pp. 9-29.

[4] EC, "DIRECTIVE 2009/28/EC OF THE EUROPEAN PARLIAMENT AND OF THE COUNCIL," *Official Journal of the European Union,* 23 April 2009.

[5] P. McKendry, "Energy production from biomass (part1," *Bioresource technology,* no. 83, pp. 37-46, 2001.

[6] BP, "Statistical Review of World Energy," 2007. [Online]. Available: https://www.bp.com/en/global/corporate/energy-economics/statistical-review-of-world-energy.html.

[7] ACS, "12 Design Principles of Green Chemistry," [Online]. Available: https://www.acs.org/content/acs/en/greenchemistry/principles/12-principles-of-green-chemistry.html.

[8] C. P. Casey, S. W. Singer, D. R. Powel and R. K. Hayashi, *J. Am. Chem. Soc.,* vol. vol. 123, pp. pp. 1090-1100, 2001.

[9] F. H. Isikgora and C. R. Becer, *Polym. Chem.,* vol. 6, p. 4497, 2015.

[10] "Wikipedia," [Online]. Available: INSERIRE URL.

[11] M. T. Holtzapple, "Encyclopedia of Food Sciences and Nutrition," p. 3060–3071, 2003.

[12] Wesleyan economics students, "Bio-energy," 5 April 2012. [Online].

[13] H. Ohara, "Biorefinery," *Appl. Microbiol Biotech.,* vol. 62, pp. 474-477, 2003.

[14] F. Cherubini, "the Biorefinery concept," *Elsevier,* vol. 51, pp. 1412-1421, 2010.

[15] P. Bhaumik and P. L. Dhepe, "Conversion of Biomass into Sugars," in *Biomass*

Sugars for Non-Fuel Applications , Dmitry Murzin, Olga Simakova, 2015, pp. 1-43.

[16] P. Kumar, D. M. Barret, M. J. Delwiche and P. Stroeve, *Ind. Eng. Chem. Res,* no. 48, pp. 3713-3729, 2009.

[17] Y. Sun and J. Cheng, *Bioresour. Technol.,* vol. 83, pp. 1-11, 2002.

[18] Q. Zhang, M. Benoit, K. De Oliveira Vigier, J. Barrault, G. Jegou, M. Philippe and F. Jerome, *Green Chem.,* no. 15, pp. 963-969, 2013.

[19] H. Ooshima, K. Aso, Y. Harano and T. Yamamoto, *Biotechnol. Lett.,* vol. 6, pp. 289-294, 1984.

[20] L. Olsson, M. Galbe and G. Zacchi, "Pretreatment of Lignocellulosic Materials for Efficient Bioethanol Production," in *Biofuels*, vol. 108, Springer Berlin Heidelberg, 2007, pp. 41-65.

[21] M. T. Holtzapple, A. E. Humphrey and J. D. Taylor, *Biotechnol. Bioeng,* vol. 33, pp. 207-210, 1989.

[22] G. Yu, S. Yano, H. Inoue, T. Endo and S. Sawayama, "Pretreatment of rice straw by a hot-compressed water process for enzymatic hydrolysis," *Applied Biochemistry and Biotechnology,* vol. 160, no. 2, pp. 539-551, 2010.

[23] Y. Kim, N. S. Mosier and M. R. Ladisch, "Enzymatic digestion of liquid hot water pretreated hybrid poplar," *Biotechnology Progress,* vol. 25, no. 2, pp. 340-348, 2009.

[24] S. P. S. Chundawat, B. Venkatesh and B. E. Dale, "Effect of particle size based separation of milled corn stover on AFEX pretreatment and enzymatic digestibility," *Biotechnology and Bioengineering,* vol. 96, no. 2, pp. 219-231, 2007.

[25] G. Brodeur, E. Yau, K. Badal, J. Collier, K. B. Ramachandran and S. Ramakrishnan, "Chemical and Physicochemical Pretreatment of Lignocellulosic Biomass: A Review," *Enzyme Research ,* 2011.

[26] T. H. Kim, Y. Y. Lee, C. Sunwoo and S. K. Jun, "Pretreatment of corn stover by low-liquid ammonia recycle percolation process," *Applied Biochemistry and Biotechnology,* vol. 133, no. 1, pp. 41-57, 2006.

[27] T. H. Kim and Y. Y. Lee, "Pretreatment and fractionation of corn stover by

ammonia recycle percolation process," *Bioresource Technology,* vol. 96, no. 18, pp. 2007-2013, 2005.

[28] J. McHardy and S. P. Sawan, "Supercritical Fluid Cleaning: Fundamentals, Technology and Applications," *Noyes Publications,* 1998.

[29] S. McIntosh and T. Vancov , "Enhanced enzyme saccharification of Sorghum bicolor straw using dilute alkali pretreatment," *Bioresource Technology,* vol. 101, no. 17, pp. 6718-6727, 2010.

[30] D. L. Sills and J. M. Gossett, "Assessment of commercial hemicellulases for saccharification of alkaline pretreated perennial biomass," *Bioresource Technology,* vol. 102, no. 2, p. 1389–1398, 2011.

[31] H. Wang, J. Wang, Z. Fang, X. Wang and H. Bu, "Enhanced bio-hydrogen production by anaerobic fermentation of apple pomace with enzyme hydrolysis," *International Journal of Hydrogen Energy,* vol. 35, no. 15, p. 8303–8309, 2010.

[32] Y. H. P. Zhang, S. Y. Ding and J. R. Mielenz , "Fractionating recalcitrant lignocellulose at modest reaction conditions," *Biotechnology and Bioengineering,* vol. 97, no. 2, p. 214–223, 2007.

[33] M. E. Himmel, W. S. Adney and J. O. Baker, "Advanced bioethanol production technologies: a perspective," *Fuels and Chemicals from Biomass,* vol. 666, pp. 2-45, 1997.

[34] C. Martìn, H. B. Klinke and A. B. Thomsen, "Wet oxidation as a pretreatment method for enhancing the enzymatic convertibility of sugarcane bagasse," *Enzyme and Microbial Technology,* vol. 40, no. 3, p. 426–432, 2007.

[35] A. B. Bjerre, A. B. Olesen, T. Fernqvist, A. Ploger and A. S. Schmidt, "Pretreatment of wheat straw using combined wet oxidation and alkaline hydrolysis resulting in convertible cellulose and hemicellulose," *Biotechnology and Bioengineering,* vol. 49, no. 5, p. 568–577, 1996.

[36] N. Sun, H. Rodriguez, M. Rahman and R. D. Rogers , ""Where are ionic liquid strategies most suited in the pursuit of chemicals and energy from lignocellulosic biomass?," *Chemical Communications,* vol. 47, no. 5, p. 1405–1421, 2011.

[37] Y. P. Zhang and L. R. Lynd, *Biotech. and Bioeng.,* vol. 88, 2004.

[38] Y. Yan and G. Jiang, *J. Biobased Mater. Bionergy,* vol. 8, pp. 553-569, 2014.

[39] A. O. Converse and H. E. Grethlein, *Chem. Eng. Ed. Fall.,* p. 186, 1984.

[40] D. W. Hwang, S. Lee, M. Seo and T. D. Chung , *Anal. Chim. Acta,* vol. 1033, pp. 1-34, 2018.

[41] P. A. Shaffer and T. E. Friedemann, *J. Biol. Chem,* vol. 86, pp. 345-374, 1930.

[42] R. M. Lederkremer and C. Marino, *Advvance in Carbohydrate Chem. and Biochem.,* vol. 58, pp. 200-281, 2003.

[43] L. P. S. Vandenberghe and C. R. Soccol, *Current Developments in Biotechnology and Bioengineering,* pp. 415-434, 2018.

[44] A. M. Canete-Rodríguez, I. M. Santos-Duenas, J. E. Jiménez-Hornero, A. Ehrenreich, W. Liebl and I. García-García, *Porcess Biochemistry,* vol. 51, p. 1891–1903, 2016.

[45] *EUROPEAN PARLIAMENT AND COUNCIL DIRECTIVE No 95/2/EC,* 20 February 1995.

[46] D. K. Ahuja, L. G. Bachas and D. Bhattacharyya, *Chemosphere ,* vol. 66, pp. 2193-2200, 2007.

[47] H. D. Wilt, " H. D. Wilt," *Ind. Eng. Prod. Res. Dev.,* vol. 11, p. 370–378, 1972.

[48] P. Kundu and A. Das, *Indian J. Exp. Biol,* vol. 22, p. 279, 1984.

[49] P. Pal, R. Kumar and S. Banerjee, *Chem. Eng. Prog,* vol. 104, p. 160–171, 2016.

[50] S. Hisashi, O. Shingi and F. Shigeo, "patent 0142725,". 1987.

[51] C. Baatz and U. Pruesse, *J. Catal.,* vol. 249, pp. 34-40, 2007.

[52] S. Biella, L. Prati and M. Rossi, *J. Catal.,* vol. 206, pp. 242-247, 2002.

[53] U. P. A. Mirescu, *Appl. Catal. B Environ.,* vol. 70, pp. 644-652, 2007.

[54] F. H. Isikgora and C. R. Becer, *Polym. Chem.,* vol. 25, pp. 1-50, 2015.

[55] L. Li, X. Jianhua, H. Jianxin and J. Han, *Environ. Sci. Technol.,* vol. 48, pp. 5290-5297, 2014.

[56] C. Weber, C. Brückner, S. Weinreb, C. Lehr, C. Essl and E. Boles, *Appl. Environ. Microbiol.,* vol. 78, pp. 8421-8430, 2012.

[57] " Rivertop Renewables, Market wired," 7 October 2015. [Online]. Available: http://www.marketwired.com/pressrelease/rivertopr-renewables-begins-commercial-production-of-rioser-detergentbuilder-2061934.htm.

[58] " Rennovia, Markets: Enabling Biobased Nylons, Polyurethanes, Plasticizers, and other sustainable materials," [Online]. Available: http://www.rennovia.com/markets/.

[59] "Biorefineries-blog:biorefineries-bioproducts," December 2015. [Online]. Available: https://biorrefineria.blogspot.com/2015/12/glucaric-acid-biorefineries.html.

[60] W. N. Haworth and W. G. M. Jones, *J. Chem. Soc.,* pp. 65-76, 1944.

[61] C. L. Rist and E. a. C. Mehltretter, *Agric. and Food Chem.,* vol. 1, pp. 779-783, 1953.

[62] K. Saeed, P. Priecel and J. A. Lopez-Sanchez, *Chimica oggi,* vol. 35, pp. 7-11, 2017.

[63] C. L. Mehltretter, C. E. Rist and B. H. Alexander, "U.S. Patent 2,472,168". 1949.

[64] J.-F. Thaburet, N. Merbouh, M. Ibert, F. Marsais and G. Queguiner, *Carbohydr. Res.,* vol. 330, pp. 21-29, 2001.

[65] N. Merbouh, J. M. Bobbitt and C. Brückner, *Carbohydr. Chem.,* vol. 21, pp. 65-67, 2002.

[66] W. A. Schroeder, P. M. Hicks, S. C. McFarlan and T. W. Abraham, "U.S. Patent 7,326,549 B2". 2008.

[67] T. S. Moon, S.-H. Yoon, A. M. Lanza, J. D. Roy-Mayhew and K. L. Prather, *Appl. Environ. Microbiol.,* vol. 75, pp. 589-595, 2009.

[68] R. A. Marcus, *Rev. Mod. Phys,* vol. 65, pp. 599-610, 1993.

[69] R. A. Marcus , *Angew. Chem. Int. Ed.,* vol. 32, pp. 1111-1121, 1993.

[70] N. M. Marković, R. R. Adžić, B. D. Cahan and E. B. Yeager, *J. Electroanal. Chem,* vol. 377, pp. 249-259, 1994.

[71] A. P. O'Mullane, *Nanoscale,* Vols. 4012-4026, p. 6, 2014.

[72] A. Zhao, J. Masa, W. Xia, A. Maljusch, M.-G. Willinger, G. Clavel, K. Xie, R. Schlögl, W. Schuhmann and M. Muhler, *J. Am. Chem. Soc.,* vol. 136, pp. 7551-7554, 2014.

[73] J. Masa, W. Xia, I. Sinev, A. Zhao, Z. Sun, S. Grützke, P. Weide, M. Muhler and W. Schuhmann.

[74] D. Baronetto, I. M. Kodintsev and S. Trasatti, *J. Appl. Electrochem.,* vol. 24, pp.

189-194, 1994.

[75] N. M. Markovic and P. N. Ross Jr., *Surf. Science Rep.,* vol. 45, pp. 117-229, 2002.

[76] H. Dau, C. Limberg, T. Reier, M. Risch, S. Roggan and P. Strasser, *ChemCatChem,* vol. 2, pp. 724-761, 2010.

[77] B. E. Conway and T.-C. Liu, *Langmuir,* vol. 6, no. 1, pp. 268-276, 1990.

[78] W. T. Mook, M. K. Aroua and G. Issabayeva, *Renew. Sust. En.,* vol. 38, pp. 36-46, 2014.

[79] C. Comninellis , *Electrochim. Acta,* vol. 39, pp. 1857-1862, 1994.

[80] C. Comninellis and E. Plattner, *Chimia,* vol. 42, pp. 250-252, 1998.

[81] C. A. Martinez-Huitle and E. Brillas, *Appl. Catal.,* vol. 87, pp. 105-145, 2009.

[82] C. Comninellis, A. Kapalka, S. Malato, S. A. Parsons and I. Poulios, *J. Chem. Technol. Biotechnol.,* vol. 83, pp. 769-776, 2008.

[83] S. Park, H. Boo and T. D. Chung, *Anal. Chim. Acta,* vol. 46, p. 556, 2006.

[84] M. W. Hsiao, R. R. Adzic and E. G. Yeager, *J. Electrochem. Sci.,* vol. 5, pp. 1246-1301, 2010.

[85] K. E. Toghill and R. G. Compton, *Int. J. Electrochem. Sci.,* vol. 5, pp. 1246-1301, 2010.

[86] Y. B. Vasil'ev, O. A. Khazova and N. N. Nikolaeva, *J. Electroanal. Chem. Interfacial Electrochem.,* vol. 196, p. 105, 1985.

[87] L. D. Burke, *Electrochim. Acta,* vol. 39, p. 1841, 1994.

[88] C. Hui-Fang, Y. Jian-Shan, L. Xiao, Z. Wei-De and S. Fwu-Shan, *Nanotechnol.,* vol. 17, no. 9, p. 2334, 2006.

[89] H. Bode, K. Demhelt and J. Witte, *Anorg. Chem,* vol. 1, p. 366, 1969.

[90] R. S. S. Guzman, J. R. Vilche and A. J. Arvia, *J. Appl. Electrochem,* vol. 8, p. 67, 1978.

[91] M. Fleischmann, K. Korinek and D. Pletcher, *J. Electroanal. Chem.,* vol. 31, p. 39, 1971.

[92] P. Oliva, J. Leonardi, J. F. Laurent, C. Delmas, J. J. Braconnier, M. Figlarz, F. Fievet and A. D. Guibert, *J. Power Sources,* vol. 8, p. 229, 1982.

[93] D. S. Hall, D. J. Lockwood and C. Bock, *Proc. R. Soc. A.,* vol. 471, pp. 1-65, 2015.

[94] K. E. Toghill, L. Xiao, N. R. Stradiotto and R. G. Compton, *Electroanal.,* vol. 22, p. 491, 2010.

[95] Q. Yi, W. Huang, W. Yu, L. Li and X. Liu, *Electroanal.,* vol. 20, p. 2016, 2008.

[96] S. Kerzenmacher, J. Ducree, R. Zengerle and F. von Stetten , *J. Power Sources,* vol. 182, pp. 66-75, 2008.

[97] J. T. C. Barragan, S. Kogikoski Jr., E. T. da Silva and L. T. Kubota, *Anal. Chem,* vol. 90, pp. 3357-3365, 2018.

[98] D. Bin, H. Wang, J. L, H. W. Z. Yin, J. Kang, B. He and Z. Li, *Electrchim. Acta,* vol. 130, pp. 170-178, 2014.

[99] W. Zhu, R. Zhang, F. Qu, A. M. Asiri and X. Sun, *ChemCatChem,* vol. 9, pp. 1721-1743, 2017.

[100] D. Bin, H. Wan, J. Li, H. Wang, Z. Yin, J. Kang, B. He and Z. Li, *Electrchim. Acta,* vol. 130, pp. 170-178, 2014.

[101] A. G. M. d. Silva, T. S. Rodrigues and S. J. Haigh, *Chem. Commun.,* vol. 53, pp. 7135-7148, 2017.

[102] L. Bicelli, B. Bozzini, C. Mele and L. A. D'Urzo, *Int. J. Electrochem. Sci.,* vol. 3, pp. 356-408, 2008.

[103] P. H. Ho, E. Scavetta, F. Ospitali, D. Tonelli, G. Fornasari, A. Vaccari and P. Benito, *Appl Clay Sci,* vol. 151, pp. 109-117, 2018.

[104] P. H. Ho, M. Monti, E. Scavetta, D. Tonelli, E. Bernardi, L. Nobili, G. Fornasari, A. Vaccari and P. Benito, *Electrochim. Acta,* vol. 222, pp. 1335-1344, 2016.

[105] K. D. Vernon-Parry, *Ill-Vs Review,* vol. 13, no. 4, pp. 40-44, 2000.

[106] P. Rostron, S. Gaber and D. Gaber, *Int. J. Res. Eng. Technol.,* vol. 6, no. 1, pp. 50-64, 2016.

[107] Y. Waseda, E. Matsubara and K. Shinoda, X-Ray Diffraction Crystallography, Springer, 2011.

[108] Y. Deng, A. D. Handoko, Y. Du, S. Xi and B. S. Yeo, *ACS Catal,* vol. 6, pp. 2473-2481, 2016.

[109] N. Mironova-Ulmane, A. Kuzmin, I. Steins, J. Grabis, I. Sildos and M. Pärs,

"Raman scattering in nanosized nickel oxide NiO," in *Conference Series 93*, 2007.

[110] D. S. Hall, D. J. Lockwood, C. Bock and B. R. MacDougall, *Proc. R. Soc.,* vol. 471, pp. 1-65, 2015.

[111] N. Pal, B. Saha, S. K. Kundhu, A. Bhaumik and S. Banerjee, *New J. Chem,* vol. 39, pp. 8035-8043, 2015.

[112] C. Z. Zhao, C. L. Shao, M. H. Li and K. Jiao, *Talanta,* vol. 71, pp. 1769-1773, 2007.

[113] Y. Vlamidis, S. Fiorilli, M. Giorgetti, I. Gualandi and E. Scavetta, *RSC Adv,* vol. 6, p. 976_985, 2016.

[114] I. Danaeea, M. Jafariana, F. Forouzandeha, F. Gobal and M. Mahjani, *Electrochimica Acta , vol. 53, pp. 6602-6609, 2008,* vol. 53, pp. 6602-6609, 2008.

[115] A. Shimizu, K. Tanaka and M. Fujimori , *Chemosphere ± Global Change Science* , vol. 2, pp. 425-434, 2000.

[116] D. W. Hwang, S. Lee, M. Seo and T. D. Chung, *Anal. Chim. Acta,* vol. 1033, pp. 1-34, 2018.